2016

Wide Field Measurements Using A Spatial Heterodyne Raman Spectrometer For Transmission Raman Spectroscopy And Standoff Detection

Kimberly A. Fessler
University of South Carolina

WIDE FIELD MEASUREMENTS USING A SPATIAL HETERODYNE RAMAN SPECTROMETER FOR TRANSMISSION RAMAN SPECTROSCOPY AND STANDOFF DETECTION

by

Kimberly A. Fessler

Bachelor of Science
East Carolina University, 2008

Master of Science
University of Manchester, 2010

Submitted in Partial Fulfillment of the Requirements

For the Degree of Doctor of Philosophy in

Chemistry

College of Arts and Sciences

University of South Carolina

2016

Accepted by:

S. Michael Angel, Major Professor

Stephen L. Morgan, Committee Member

Michael L. Myrick, Committee Member

Geoffrey I. Scott, Committee Member

Lacy Ford, Senior Vice Provost and Dean of Graduate Studies

DEDICATION

In memory of Larry B. Blalock, my Pawpaw. Thank you for building me up as a person and teaching me there are no limits.

ACKNOWLEDGEMENTS

I would like to thank Dr. Angel for turning a topic I hated into a topic I love. It takes a special kind of teacher to make that happen.

To my family, especially my mother, I want to say thank you for all the support and encouragement. To my husband, Brett, thank you for being there for me and helping me make it through this process.

ABSTRACT

Our group recently developed a new type of Fourier transform Raman spectrometer, the spatial heterodyne Raman spectrometer (SHRS), for planetary exploration. The SHRS is a high spectral resolution, high throughput, compact dispersive interferometer, similar in design to a Michelson interferometer, where the mirrors are replaced by stationary diffraction gratings. The SHRS has no moving parts and does not require an entrance slit, making the throughput of the system orders of magnitude larger than a typical dispersive spectrometer. The wide field-of-view (FOV) of the SHRS enables wide area measurements without loss of sensitivity or spectral resolution and offers advantages such as minimizing sample photodegradation by using large laser spots on the sample and easy coupling to a telescope for standoff Raman. The lack of moving parts and compactness of the SHRS makes the system lightweight and robust, which is ideal for a deployable standoff detection instrument intended for planetary exploration. Our group has demonstrated visible and UV measurements using the SHRS in bench-top and standoff configurations; however, there are no published quantitative studies measuring the FOV of the SHRS for standoff Raman or the laser irradiance necessary to reduce photodegradation. The work presented quantifies the FOV, beam diameter and irradiance required to reduce photodegradation, and demonstrates 1D imaging using wide area illumination. A prism-based SHRS was also investigated and preliminary results are discussed.

The wide FOV and high throughput of the SHRS makes the system well suited for transmission Raman spectroscopy (TRS). In TRS, the laser is brought in from the backside of the sample, and Raman photons are collected on the opposite side after diffusely scattering through the sample. The diffuse scattering of light increases interactions within the sample leading to spectra that are more representative of the bulk. However, the Raman scattered photons exit the sample over a very large area, and the dispersive Raman spectrometers typically used in TRS suffer sensitivity losses, in comparison to backscatter Raman, due to low collection efficiency resulting from the narrow spectrometer slit. TRS measurements using the SHRS are demonstrated and comparisons to a more conventional, high throughput dispersive spectrometer are discussed.

TABLE OF CONTENTS

DEDICATION iii

ACKNOWLEDGEMENTS iv

ABSTRACT v

LIST OF FIGURES viii

CHAPTER 1: INTRODUCTION 1

CHAPTER 2: CHARACTERIZATION OF A VISIBLE SPATIAL HETERODYNE RAMAN SPECTROMETER (SHRS) FOR STANDOFF DETECTION 26

CHAPTER 3: TRANSMISSION RAMAN MEASUREMENTS USING A SPATIAL HETERODYNE RAMAN SPECTROMETER (SHRS) 55

CHAPTER 4: ALL-REFRACTIVE SPATIAL HETERODYNE RAMAN SPECTROMETER (SHRS): PRELIMINARY RESULTS 79

REFERENCES 97

APPENDIX A: PERMISSION TO REPRINT 107

LIST OF FIGURES

Figure 1.1 Energy-level diagram depicting: a. Rayleigh scattering, b. Stokes and c. anti-Stokes. E_ι, E_R, and E_υ are the energies of the laser, Raman scattering, and vibrational mode, respectively. 14

Figure 1.2 Schematic of SHRS. S is the incoming signal, L_1 & L_2 are Lenses, BS is the beam splitter, G_1 & G_2 are gratings, and the CCD is the detector. The Littrow angle is θ_L, and F are laser-blocking and bandpass filters. 15

Figure 1.3 Raman spectrum of potassium perchlorate measured using the SHRS, along with the corresponding fringe pattern image and fringe pattern cross section produced by binning the columns. 16

Figure 1.4 Standoff Raman spectroscopy schematic. The laser light is directed to the sample using mirrors M_1 and M_2, and the Raman scattered light is collected by a telescope and directed into a spectrometer using a coupling lens..... 17

Figure 2.1 SHRS schematic- The Raman light collected by L_1 is focused down and re-collimated by L_2 and directed into the entrance aperture (A.). The light is split 50/50 by the beam splitter (BS). The gratings (G) disperse the light back towards the beam splitter, where the wavefronts recombine. The imaging lens (I) images the gratings onto the CCD detector. SF is a spatial filter, variable in size, used in some of the experiments..... 42

Figure 2.2 Raman spectra and corresponding fringe cross sections of rock samples measured with the SHRS using a 2 W, 532 nm laser at 4.5 m. The top two spectra, calcite (a.) and quartz (b.), were measured for 30 sec. acquisition time. The lower two spectra, gypsum (c.) and olivine (d.), were measured for 60 sec. and 90 sec. acquisition time, respectively. 43

Figure 2.3 Raman spectra of solid sodium sulfate (top) and a 2.2 x 10^{-3} M sodium sulfate solution measured with the SHRS as a liquid (lower) and frozen at 77 K (middle), offset for clarity. Spectra measured for 90 and 30 second acquisition times for the solutions and solid, respectively, using 532 nm laser at ~2 W power. 44

Figure 2.4 Plot of Raman intensity of the 219 cm^{-1} sulfur band as beam diameter is increased from ~200 mm to ~50 mm. The Raman spectra were measured with a 532 nm laser at 200 mW for a 10 sec. acquisition time. The upper right inset are the Raman spectra of sulfur, one spectrum for each beam size measured. 45

Figure 2.5 Plot of the Raman intensity of potassium perchlorate (triangles, left axis) and sodium sulfate (circles, right axis) as the laser is moved away from optical axis. Inset is Raman spectra of potassium perchlorate (lower) and sodium sulfate (top), offset for clarity. Raman spectra of potassium perchlorate in a 1 cm cuvette were measured using a 532 nm laser at ~700 mW for 15 sec. acquisition time. Raman spectra of a 10 cm diameter sodium sulfate sample were measured using a 532 nm laser at ~1.5 W for 30 sec. acquisition time. 46

Figure 2.6 Plot of the Raman intensity of the 219 cm^{-1} sulfur band as laser power is varied using various laser beam diameters. The 0.25 (triangle) and 3 (diamond) mm beams presented signs of photodegradation, but the 19 (square) and 64 (circle) mm beams were free of photodegradation. Plots offset for clarity. 47

Figure 2.7 Raman spectra using a cylindrical lens for imaging and a collimated input beam for non-imaging were measured using ~1.15 W, 532 nm laser power illuminating the sample with a 3.5-4 cm beam diameter. The sample consisted of three vertically stacked 1 cm cuvettes containing $KClO_4$, NH_4NO_3, and a $NaNO_3/NaNO_2$ mixture. The Raman spectra labeled Cylindrical Rows 1-3 correspond to the three distinct rows in CCD image on the right measured with the cylindrical lens (a.). The Raman spectrum labeled Collimated corresponds to the CCD image on the right measured with the collimated beam (b.). 48

Figure 3.1 SHRS schematic- The Raman light collected by L_1 is directed through the filters (F) and into the input aperture (I), and the light is split 50/50 by the beam splitter (BS). The gratings (G) disperse the light and send it back towards the beam splitter, where the beams recombine. The imaging lens (L_2) focuses the image plane onto the CCD detector. Kaiser Holospec f/1.8 dispersive spectrometer- The Raman scatter is collected with the collection lens (L_1), which collimates the light. The coupling lens (L_2) focuses the collimated light into the entrance slit (A) of the spectrometer. a. Transmission Raman geometry. b. Backscatter Raman geometry. 69

Figure 3.2 Transmission Raman spectra of acetaminophen, ammonium nitrate, a sodium nitrate/sodium nitrite mixture, and potassium perchlorate (from top to lower). The salts were measured in 1 cm cuvettes using 10 seconds acquisitions with a 1 W, 532 nm laser, and the acetaminophen tablet was measured using 90 seconds acquisition with ~200 mW laser power. Spectra offset for clarity. The fringe image cross sections are inset in the upper left hand corner and the order is identical to the spectra. The acetaminophen fringe cross section was background subtracted before generating the Raman spectrum..... 70

Figure 3.3 Transmission (lower) and backscatter (top) Raman spectra of ibuprofen pellet (4.4 mm thick, 13 mm diameter) measured with the SHRS using 60 second acquisition time and 460 mW. The backscatter spectrum was offset for clarity..... 71

Figure 3.4 Width of the area viewed, showing Raman intensity versus position of razor edge, measured using a 250 mm focal length lens as the collection optic for the SHRS

(circles) and f/1.8 dispersive spectrometer (squares). A $KClO_4$ sample was used for these measurements. The sample thickness was 10 x 10 mm for the SHRS experiment and 7 x 13 mm for the dispersive experiment. 72

Figure 3.5 Width of the area viewed, showing Raman intensity versus position of razor edge, measured using a 50.8 mm focal length lens as the collection optic for the SHRS (circles) and f/1.8 dispersive spectrometer (squares). A 7 x 13 mm $KClO_4$ pellet was used for these measurements. 73

Figure 3.6 Transmission Raman spectra of ibuprofen measured with the f/1.8 dispersive spectrometer (lower) and the SHRS (top). Five replicate measurements with each spectrometer are shown. The ratio of replicate measurements is shown for the SHRS (solid line) and the dispersive spectrometer (dashed line). Inset: shows the SHRS spectrum corrected for CCD gain (i.e. intensity x 4), as well as a dispersive spectrum, over the full spectral range. The spectra were measured with 200 mW laser power using100 second acquisition time and a 250 mm focal length lens. 74

Figure 4.1 Schematic and images of proto-types built in our lab of an all-refractive SHRS in a mirror coated prism configuration (a.) and a prism mirror pair configuration (b.). S is the incoming signal, L_1 & L_2 are Lenses, BS is the beam splitter, P_1 & P_2 are prisms, M_1 & M_2 are mirrrors, and the CCD is the detector. The Littrow angle is θ_L, and F are laser-blocking and bandpass filters 88

Figure 4.2 Schematic of order overlap (a.) and an image showing order overlap. Image is a fringe image recorded on the CCD in a grating-based SHRS system. 89

Figure 4.3 Schematic of dispersion in a prism showing the (a.) angle of deviation, δ, and (b.) a prism set to minimum deviation for blue light. Light blue dotted line is the normal to prism face, γ_i is the incident angle, and γ_f is the exit angle. 90

Figure 4.4 Schematic showing the dispersion through the prism. Angle of incidence (γ_L) and apex angle (α). 91

Figure 4.5 Emission spectrum from low pressure Hg lamp measured for 500 msec using the coated-prism all-refractive SHS set at 532 nm Littrow wavelength. Inset is a spectrum of a 20 nm broadband source (white light lamp filtered by a 558 nm bandpass filter) measured for 10 msec. acquisition time. 92

Figure 4.6 Raman spectrum of CCl_4 measured for 60 sec using the coated-prism all-refractive SHS set at 532 nm Littrow wavelength. 93

Figure 4.7 Emission spectrum from low pressure Hg lamp measured for 30 sec. acquisition time using the prism-mirror pair all-refractive SHS set at 532 nm Littrow wavelength. Inset is a same spectrum with y-axis scale change to show 576.9 and 579 nm emission lines. 94

Figure 4.8 Illustration of the wedge prism (a) showing the rotation in the xy plane that affects the path difference in the two arms of the interferometer and (b.) showing the dimensions of the prism from a side view. 95

CHAPTER 1

INTRODUCTION

1.1 Raman Spectroscopy

Raman spectroscopy is a type of inelastic molecular scattering discovered by C.V. Raman in 1928[1], which probes the vibrational/rotational modes of a molecule. When a molecule is excited by a light source, the interaction between the molecule and light produce several scattering events that provide structural information about the molecule, often best represented by an energy-level diagram (Figure 1.1). If the molecule is much smaller than the excitation wavelength, two types of scattering can occur, elastic and inelastic. Rayleigh scattering is elastic scattering that results from the molecule emitting a photon of the same energy as the exciting photon; most photons are Rayleigh scattered. However, approximately one out of 10^7 photons interacting with a molecule are inelastically scattered, which is referred to as Raman scattering.

In Raman scattering the energy of the scattered photon, (E_R), is the energy difference between the exciting photon, (E_l), and the energy of an excited vibrational mode, (E_v). The energy of the scattered photon can be of greater (anti-Stokes) or lower (Stokes) energy than that of the excitation photon. A photon is Stokes Raman scattered when the molecule is excited from the ground state to a virtual state followed by emission of a lower energy photon, leaving the molecule in an excited vibrational level of the ground electronic state. In anti-Stokes Raman scattering, the molecule is excited from an excited vibrational level in the ground electronic state to a virtual state before emitting a photon of higher energy, as the molecule returns to the ground vibrational state.

In a typical Raman experiment, the sample is irradiated with a laser, and the scattered light is collected and analyzed using a spectrometer. The Raman signal (S_R) detected is governed by Equation 1.1.

$$S = (PN_m\sigma_R)(\varepsilon TQt) \qquad \text{Equation 1.1}$$

where P is the laser intensity, N_m is the number of molecules, σ_R is the Raman cross-section of the molecule, ε is the spectrometer collection solid angle, T is the transmission of the optics, Q is the detector efficiency, and t is acquisition time. The first three variables are dependent upon the characteristics of the molecule and laser, while the latter are related to the characteristics of the spectrometer and collection optics.

Lasers are typically used as the excitation source for Raman measurements to deliver a large number of monochromatic photons to a small area of the sample. The magnitude of the Raman cross-section, usually on the order of 10^{-27} cm^2/sr, is related to the polarizability of the molecule. Polarizability is determined by the probability of the excitation light inducing a dipole in the molecule. The Raman signal is also proportional to the laser frequency (υ_{ex}) by υ_{ex}^4, which means ultra violet (UV) wavelengths produce higher signals than visible or near-infrared wavelengths. However, the larger signal obtained by using higher energy lasers can be offset by photodegradation of the sample.

The characteristics of the collection optics and spectrometer are also important aspects to consider when using Raman spectroscopy. The transmission properties of the collection and spectrometer optics can greatly reduce the Raman signal if not chosen correctly. The optics should be optimized to transmit light efficiently in the wavelength region of the collected light. For some wavelength regions, such as the deep UV, high

quality optics are not readily available. Besides reduced transmission, poor quality optics can also introduce errors as the light travels through the optic, such as wavefront distortion, chromatic aberrations, and spherical aberrations. These can be problematic for interferometer based spectrometers.

The spectrometer collection efficiency (i.e., throughput or Etendue) determines how much light can be collected and transferred to the detector. The Etendue of a spectrometer is a function of area viewed (A) and collection solid angle (Ω, steradians (sr)) of the limiting aperture.

$$\varepsilon = \Omega A \qquad \text{Equation 1.2}$$

Detector efficiency is another important part of the spectroscopic system. In fact, Raman spectroscopy became more useful as an analytical technique after charge coupled devices (CCD) were used for Raman spectroscopy[2,3] due to improved sensitivity and signal-to-noise ratios, multiwavelength detection, and faster acquisition times.[4]

The two most commonly used types of Raman spectrometers are slit-based dispersive and Fourier transform (FT) systems. Each type of spectrometer has advantages and disadvantages, and the specific application requirements will determine the more suitable spectrometer. Dispersive spectrometers separate the input wavelengths by using a light-dispersing grating, and the resolution is a function of the grating dispersion and slit width. In a dispersive Raman spectrometer, the slit width is typically 25 - 100 μm for moderate resolution, ~5-10 cm^{-1}, capable of resolving most Raman bands. The narrow slit width in a dispersive spectrometer limits the Etendue of the system, as well as the viewable area of the sample.

FT Raman using a near infrared laser was shown to provide fluorescence free Raman spectra, which increased the applicability of Raman spectroscopy to chemical analysis of "real world" samples and revolutionized Raman spectroscopy as a technique for analytical applications .[4-6] The initial FT Raman spectrometers were modified FTIR spectrometers, which are Michelson interferometers. In a Michelson interferometer, light is split 50/50 at the beam splitter into two arms, one with a stationary mirror and the other with a moving mirror. The wavelengths are measured by the constructive and destructive interference generated from phase changes as the moving mirror travels, and the spectral resolution depends on the maximum mirror travel. Therefore, the spectral resolution of FT spectrometers does not depend on a slit and the entrance aperture can be large, increasing the Etendue in comparison to a dispersive spectrometer. However, the system requires moving parts to record a spectrum.

1.2 Spatial Heterodyne Raman Spectroscopy

Spatial heterodyne spectroscopy was originally developed and described by J. Harlander for emission measurements.[7] Our group recently adapted the spatial heterodyne spectrometer to Raman measurements.[8] The spatial heterodyne Raman spectrometer (SHRS) is based on a dispersive interferometer, similar to a Michelson interferometer, with the mirrors replaced by stationary diffraction gratings, Figure 1.2. Thus the SHRS has no moving parts and does not require an entrance slit, making the optical Etendue (ε, Equation 1.2) of the system much larger than that of a conventional dispersive spectrometer.

As shown in Figure 1.2, the collected light is collimated into the SHRS, split by a 50/50 beam splitter, and directed towards the diffraction gratings. The gratings are set to the Littrow angle, the angle at which a selected wavelength retro-reflects, typically set to the laser wavelength. Light at any other wavelength is diffracted by the grating at an angle, producing a wavelength dependent crossing angle of the beam wavefronts. The superposition of the diffracted beams in each arm of the interferometer forms a fringe pattern, as a result of constructive and destructive interference, which is imaged onto an imaging detector such as a CCD. The fringe spacing is defined by:

$$f = 4(\sigma - \sigma_L)\tan\theta_L \qquad \text{Equation 1.3}$$

where f is fringes per centimeter, θ_L is the Littrow angle, σ is the wavenumber of the Raman band and σ_L is the Littrow wavenumber. Equation 1.3 demonstrates all wavenumbers entering the spectrometer are heterodyned to the Littrow wavenumber, and when the Littrow wavelength corresponds to the laser wavelength, the fringe wavenumber is proportional to the Raman shift in cm^{-1}. Thus, each Raman band produces a unique set of fringes to form an interferogram and all wavelengths are measured simultaneously. The intensity of the fringe pattern is a function of position x on the detector, given by:

$$I(x) = \int_0^\infty B(\sigma)\{1 + \cos[8\pi(\sigma - \sigma_L)x\tan\theta_L]\}d\sigma \qquad \text{Equation 1.4}$$

where $B(\sigma)$ is the input spectral intensity at wavenumber σ, and the Fourier transform of $I(x)$ yields the Raman spectrum.[9-12] A fringe image of potassium perchlorate produced by

exciting the sample with a 532 nm laser and setting σ_L to 532 nm is shown in Figure 1.3, along with the image cross section and resulting Raman spectrum.

The resolving power (R_0) of the system is equal to the number of grooves illuminated on both gratings

$$R_0 = 2WG_d \qquad \text{Equation 1.5}$$

where W is the width of the diffraction gratings and G_d is the grating groove density (grooves/mm). Using the grating equation, the resolving power in Equation 1.5 can also be written in terms of the wavenumber and Littrow angle as:

$$R_0 = 4W\sigma\sin\theta_L \qquad \text{Equation 1.6}$$

Equation 1.5 highlights the importance of illuminating the entire width of the diffraction grating to achieve the highest possible resolution. The number of detector elements (N) illuminated is also important, because the SHRS spectral bandpass (BP) is limited by N/2 due to the Nyquist criterion, see equation 1.7.

$$BP = N\lambda / 2R_o \qquad \text{Equation 1.7}$$

The Nyquist criterion determines the spatial frequency that can be measured without aliasing.[9] Thus, the total number of pixels illuminated on the CCD determines the spectral range of the system, while the Littrow wavelength selects the spectral region.

As an example of a typical SHRS spectrometer used in our lab, the parameters of an SHRS designed for detection in the visible region are given and used to calculate the resolving power and bandpass. Assuming a 532 nm doubled Nd:YAG laser is used for sample excitation and to set the Littrow; a CCD camera with 1,340 pixels (N) in the

horizontal direction as the detector; and 25.4 mm square, 150 grooves/mm gratings, the calculated values described above are shown in Table 1.1.

Table 1.1: Visible SHRS Specifications

Excitation Wavelength	532 nm
CCD Dimensions	1340 × 1300 pixels
Grating Dimensions	25.4 mm × 25.4 mm
Grating Density	150 grooves/mm
Resolving Power	7620
Resolution	2.46 cm^{-1}
Bandpass	1500 cm^{-1}

When taken all together, the defining features of the SHRS design make the system a unique spectrometer with advantages over other spectrometers used for Raman measurements. The SHRS is a high spectral resolution, high throughput compact spectrometer with no moving parts. In comparison, a slit-based spectrometer needs to be large to achieve high resolution by using large gratings and long focal lengths with small slit widths, and Michelson interferometers require a moving mirror to measure spectra and must be scanned. The high Etendue of the SHRS enables wide area measurements without losing light, whereas an unfocused laser cannot be paired with a conventional dispersive spectrometer due to considerable light loss at the slit. The lack of moving parts and compactness of the SHRS makes the system lightweight and robust, which is ideal for a deployable instrument for applications such as standoff detection or in-line process monitoring.

1.3 SHRS for Standoff Raman Applications and Current Progress

Standoff Raman spectroscopy has been shown to be a useful technique for a wide range of applications such as art and archeology,[13] forensics and homeland security applications,[14-15] and planetary exploration.[16-17] The well-defined spectral features in Raman spectra allow for unambiguous identification of molecules in homogeneous and heterogeneous samples of solids, liquids, and gases, which is useful for in situ measurements.[18] Using standoff configuration for Raman measurements allows for analysis of inaccessible samples or highly dangerous compounds at safe distances. The SHRS was developed and demonstrated by our group in 2011 as a novel spectrometer suitable for standoff Raman spectroscopic measurements for planetary applications.[8]

A typical standoff Raman experiment is performed by using a laser to illuminate a sample at a distance, ~tens to hundreds of meters, and the Raman scattered light is collected by a telescope and directed into a spectrometer, see Figure 1.4. Standoff Raman was first described and demonstrated for atmospheric gas measurements,[19-22] and was later extended to measurements of inorganic and organic compounds using a portable Raman standoff system developed for radioactive wastes analysis in underground storage tanks.[23] Other recent advances in standoff Raman spectroscopy include: remote measurements up to 1500 m[24]; systems designed for planetary exploration[16-17,25-26] and explosives detection[15,27-29]; gated detection for ambient light operations[30-31]; and systems developed to take advantage of the resonance enhancement and higher Raman cross sections in the deep-UV.[27,32-38]

Excitation at deep-UV wavelengths has been shown to provide Raman spectra free from interference of longer wavelength fluorescence, which often plagues visible

wavelength Raman measurements.[39] However, UV excited standoff Raman measurements require a high resolution spectrometer capable of resolving the closely spaced Raman bands observed in a narrow spectral range, and care must be taken to avoid laser-induced photodegradation by utilizing low laser irradiance. Spectrometers with sufficiently high spectral resolution for deep-UV Raman typically require large, high dispersion gratings and long focal length optics, making the spectrometer large with low light throughput. Therefore, conventional dispersive spectrometers will lose sensitivity when using large laser spots or reduced laser power to reduce sample irradiance, and due to the large size, high resolution dispersive spectrometers are not ideal as portable instruments for planetary exploration.

The spatial heterodyne Raman spectrometer (SHRS) is a compact, high resolution instrument first described by Gomer et al. for visible Raman measurements,[8] and later extended for deep UV[40-41] and standoff UV Raman measurements.[42] Hu , et al have demonstrated standoff detection using the SHRS with no collection optics, as well as 2D SHRS spectra of analytes through a plastic bottle.[43-44] The SHRS has no moving parts and all wavelengths are measured simultaneously, which makes the system compatible with pulsed lasers and gated detection. The SHRS does not require an entrance slit to maintain high resolution and has a large angular field of view (FOV), making the optical Etendue of the system profoundly larger than that of a conventional dispersive spectrometer. The Etendue of the SHRS allows wide area measurements to be made without losing sensitivity or spectral resolution and sample photodegradation can be avoided by using large laser spots on the sample. For standoff Raman measurements, the large entrance aperture of the SHRS should reduce telescope alignment constraints and minimize laser

pointing stability issues, because small movements of the laser spot on the target do not reduce the amount of light collected by the spectrometer, as recently demonstrated in our lab for standoff LIBS measurements.[45] There are no published quantitative studies to measure the field-of-view (FOV) of the SHRS for standoff Raman, or the laser irradiance and associated beam diameter necessary to reduce photodegradation. The work presented in Chapter 2 quantifies the FOV (i.e. width of the area viewed), beam diameter required to reduce photodegradation of sulfur, and also demonstrates 1D imaging using wide area illumination.

1.4 Transmission Raman Spectroscopy

Transmission Raman spectroscopy (TRS) provides nondestructive, noninvasive, and unique molecular identification of the bulk contents of a heterogeneous sample.[46-47] TRS has been shown to be a useful technique in various areas of research such as cancer diagnostics,[48] pharmaceutical qualification and quantification,[49] and process control applications.[50] Stone and Matousek demonstrated the ability to distinguish between benign and malignant markers of breast cancer tumors at clinically relevant depths using TRS.[48] Eliasson et al. conducted feasibility studies using TRS for quantitative analysis of pharmaceutical samples. The work demonstrated TRS, in combination with chemometrics, could be used to measure the active pharmaceutical ingredient concentration with ~1-2% relative error despite strong Raman signals from the capsule shell.[49] Macleod and Matousek reviewed TRS studies pertaining to using TRS for process control of pharmaceutical products.[50] The review describes how TRS can be used for fast, quantitative, nondestructive process control measurements with high specificity of the bulk components for heterogeneous samples.

In TRS, the laser is brought in from the backside of the sample, and laser and Raman photons are scattered diffusely through the sample and collected on the opposite side. The TRS technique takes advantage of the diffuse scattering of Raman photons through a sample to increase the Raman signal from the bulk relative to the surface (i.e. reduced sub-sampling). Sub-sampling is the bias to surface layer constituents in backscatter Raman of highly scattering samples, which limits the ability to use backscatter Raman to obtain spectra that are representative of the bulk for highly scattering samples. In TRS, diffuse scattering of light increases interactions within the sample leading to spectra that are more representative of the bulk and can lead to reduced scattered laser light in the Raman spectrum.[46,51] However, this comes at the price of reducing the Raman signal compared to backscatter Raman.

In TRS, Raman scattered photons exit the sample in a very large area, in a spot about 6 times the sample thickness.[52-54] Typical dispersive spectrometers have small entrance slits and are not efficient at collecting light from a large area sample, which leads to low collection efficiency and reduced sensitivity in TRS in comparison to backscatter Raman. The backscatter/transmission (B/T) ratio is a measure of signal loss and is typically a large number for TRS, 10-100.[46-47,49,55] To increase the sensitivity in TRS measurements, signal enhancement techniques can be employed or the collection area can be increased. Signal enhancement has been achieved through the use of unidirectional coupling mirrors to recycle the Raman and laser photons lost on the non-collection sides of the sample.[56-57] Most TRS studies have used fiber optic bundles to increase the collection area, but the small diameter of the fibers still limits the total area that can be viewed, and typical B/T ratios using optical fibers for light collection are 10 to

18.[46-49,58] FT-Raman has also been demonstrated for TRS measurements as the throughput should be larger than a typical dispersive spectrometer. However, Pelletier et al., using FT Raman for TRS, reported a 20 -100 times decrease in the transmission Raman intensity compared to the backscatter intensity, citing self-absorption at near-infrared (NIR) wavelengths and poor Raman collection efficiency.[55]

Recently, we demonstrated a new type of Fourier transform (FT) Raman spectrometer, the spatial heterodyne Raman spectrometer (SHRS), that has very high light throughput and a wide field-of-view.[8] The SHRS is well suited for measuring large sample areas and could be useful for TRS measurements. Chapter 3 demonstrates TRS using the SHRS and to make comparisons to a more conventional, high throughput dispersive spectrometer.

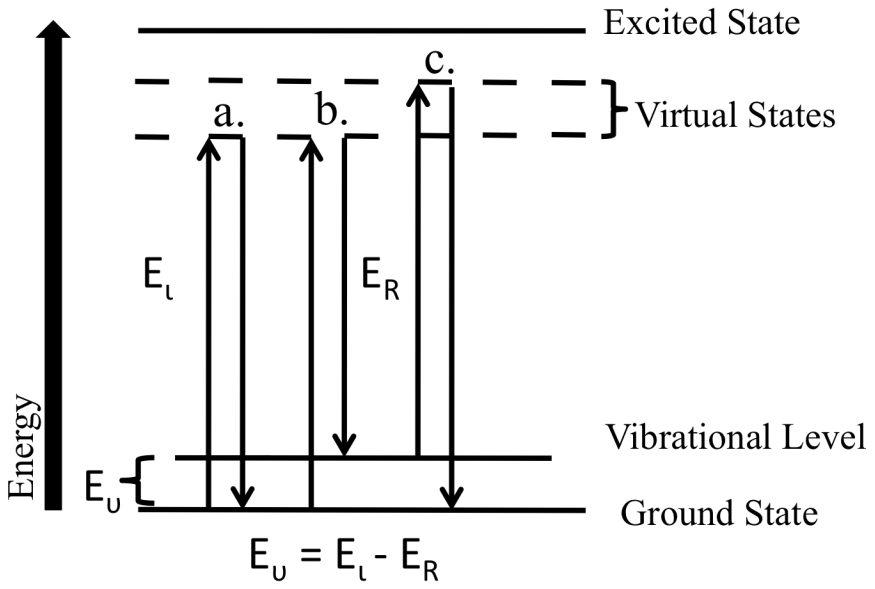

Figure 1.1: Energy-level diagram depicting: a. Rayleigh scattering, b. Stokes and c. anti-Stokes. $E_ι$, E_R, and $E_υ$ are the energies of the laser, Raman scattering, and vibrational mode, respectively.

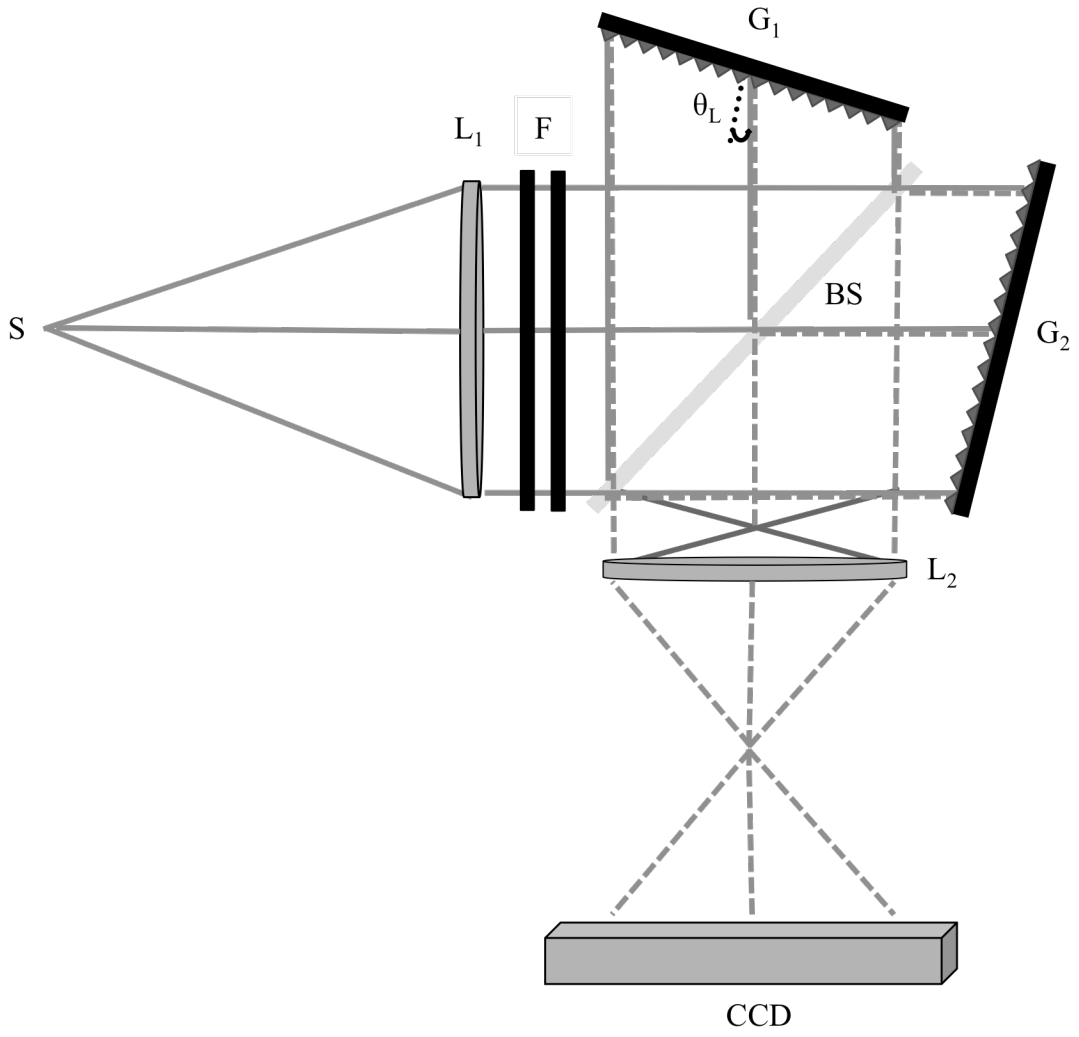

Figure 1.2: Schematic of SHRS. S is the incoming signal, L_1 & L_2 are Lenses, BS is the beam splitter, G_1 & G_2 are gratings, and the CCD is the detector. The Littrow angle is θ_L, and F are laser-blocking and bandpass filters.

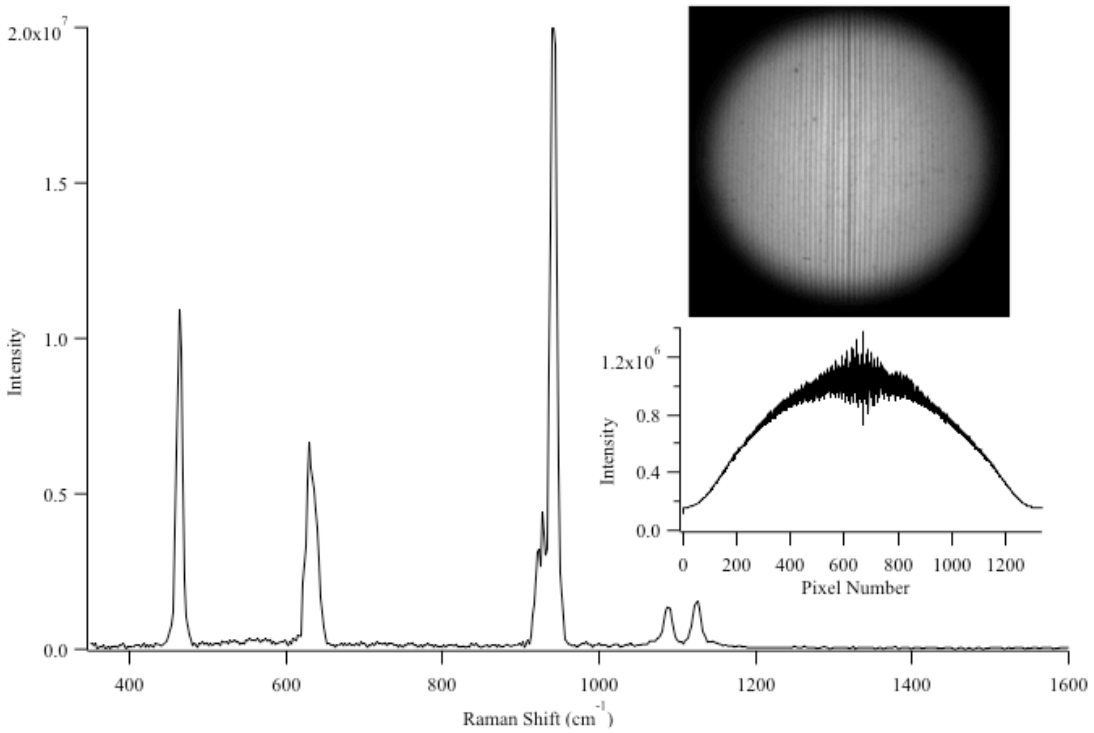

Figure 1.3: Raman spectrum of potassium perchlorate measured using the SHRS, along with the corresponding fringe pattern image and fringe pattern cross section produced by binning the columns.

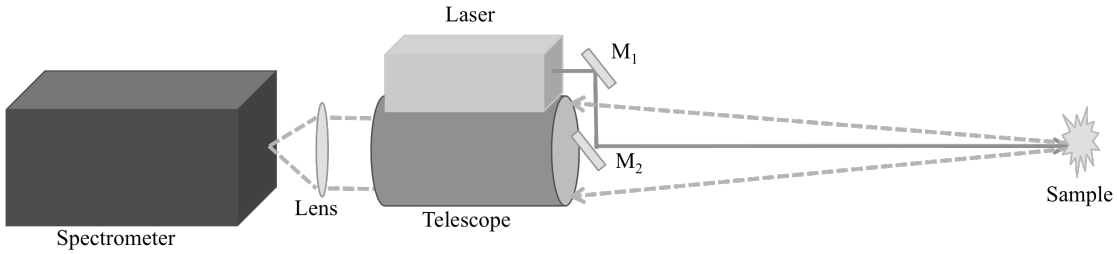

Figure 1.4: Standoff Raman spectroscopy schematic. The laser light is directed to the sample using mirrors M_1 and M_2, and the Raman scattered light is collected by a telescope and directed into a spectrometer using a coupling lens.

1.5 References

1. C.V. Raman, K.S. Krishnan. “A New Type of Secondary Radiation”. Nature. 1928. 121(3048): 501–502.
2. J.J. Laserna, editor. Modern Techniques in Raman Spectroscopy. New York, USA: Wiley, 1993.
3. R.L. McCreery. “CCD Array Detectors for Multichannel Raman Spectroscopy.” In: J. Sweedler, K. Ratzlaff, and M.B. Denton, editors. Charge Transfer Devices in Spectroscopy. New York, USA: VCH, 1994. Pp. 227-228.
4. R.L. McCreery. Raman Spectroscopy for Chemical Analysis. New York, USA: Wiley, 2000.
5. T. Hirschfeld, B. Chase. “FT-Raman spectroscopy: Development and Justification.” Appl. Spectrosc. 1986. 40(2): 133-136.
6. D.B. Chase. “Fourier Transform Raman Spectroscopy.” J. Am. Chem. Soc. 1986. 108(24): 7485-7488.
7. J.M. Harlander. Spatial Heterodyne Spectroscopy: Interferometric Performance at any Wavelength Without Scanning. [Ph.D. Thesis]. Madison, WI: University of Wisconsin, 1991.
8. N.R. Gomer, C.M. Gordon, P. Lucey, S.K. Sharma, J.C. Carter, S.M. Angel. “Raman Spectroscopy Using a Spatial Heterodyne Spectrometer: Proof of Concept.” Appl. Spectrosc. 2011. 65(8): 849-857.

9. J.M. Harlander. Spatial Heterodyne Spectroscopy: Interferometric Performance at any Wavelength Without Scanning. [Ph.D. Thesis]. Madison, WI: University of Wisconsin, 1991.
10. J.M. Harlander, F.L. Roesler, S. Chakrabarti. “Spatial Heterodyne Spectroscopy: A Novel Interferometric Technique for the FUV.” In: O.H.W. Siegmund, H.S. Hudson, editors. EUV, X-Ray, and Gamma-Ray Instrumentation for Astronomy. Proc. SPIE. 1990, 1344: 120-131.
11. J.M. Harlander, F.L. Roesler, J.G. Cardon, C.R. Englert, R.R. Conway. “Shimmer: A Spatial Heterodyne Spectrometer for Remote Sensing of Earth’s Middle Atomsphere.” Appl. Opt. 2002. 41(7): 1343-1352.
12. J. Harlander, R. Reynolds, F. Roesler. “Spatial Heterodyne Spectroscopy for the Exploration of Diffuse Interstellar Emission-Lines at Far-Ultraviolet Wavelengths.” Astrophys. J. 1992. 396(2): 730-740.
13. A.J. Hobro, B. Lendl. “Stand-off Raman Spectroscopy.” Trends Anal. Chem. 28(11): 1235-1242.
14. E.L. Izake. “Forensic and Homeland Security Applications of Modern Porable Raman Spectroscopy.” Forensic Sci. Int. 2010. 202(1-3): 1-8.
15. K.L. Gares, K.T. Hufziger, S.V. Bykov, S.A. Sanford. “Review of Explosive Detection Methodologies and the Emergence of Standoff Deep UV Resonance Raman.” J. Raman Spectrosc. 2016. 47(1): 124-141.
16. S.M. Angel, N.R. Gomer, S.K. Sharma, C. McKay. “Remote Raman Spectroscopy for Planetary Exploration: A Review.” Appl. Spectrosc. 2012. 66(2): 137-150.

17. S.K. Sharma, P.G. Lucey, M. Ghosh, H.W. Hubble, K.A. Horton. “Stand-off Raman spectroscopic Detection of Minerals on Planetary Surfaces.” Spectrochim. Acta, Part A. 2003. 59(10): 2391-2407.
18. R.S. Das, Y.K. Agrawal. “Raman Spectroscopy: Recent Advancements, Techniques and Applications.” Vib. Spectrosc. 2011. 57(2): 163-176.
19. J. Cooney. ‘‘Satellite Observations Using Raman Component of Laser Backscatter.’’ In: R. Zirkind (ed.) Proceedings of the Symposium of Electromagnetic Sensing of the Earth from Satellites. New York, NY: Polytechnic Institute of Brooklyn Press, 1967, pp. P1–P10.
20. D.A. Leonard. ‘‘Observation of Raman Scattering from the Atmosphere using a Pulsed Nitrogen Ultraviolet Laser.’’ Nature. 1967. 216(5111): 142–143.
21. T. Hirschfeld. ‘‘Range Independence of Signal in Variable Focus Remote Raman Spectrometry.’’ Appl. Opt. 1974. 13(6): 1435–1437.
22. R.M. Measures. Laser Remote Sensing: Fundamentals and Applications. New York, USA: John Wiley & Sons, 1984.
23. S.M. Angel, T.J. Kulp, T.M. Vess. ‘‘Remote-Raman Spectroscopy at Intermediate Ranges Using Low-Power CW Lasers.’’ Appl. Spectrosc. 1992. 46(7): 1085–1091.
24. R.L. Aggarwal, L.W. Farrar, D.L. Polla. ‘‘Measurement of the Absolute Raman Scattering Cross Sections of Sulfur and the Standoff Raman Detection of a 6 mm thick Sulfur Specimen at 1500 m.’’ J. Raman Spectrosc. 2011. 42(3): 461–464.

25. P.G. Lucey, T.F. Cooney, S.K. Sharma. ‘‘A Remote Raman Analysis System for Planetary Landers.’’ Paper presented at: LPSC 1998. Houston, TX; March 16–20 1998.
26. K.A. Horton, N. Domergue-Schmidt, S.K. Sharma, P. Deb, P.G. Lucey. ‘‘Remote Raman System for Planetary Landers: Data Reduction and Analysis.’’ Paper presented at: LPSC 2000.Houston, TX; March 13–17 2000.
27. M. Gaft, L. Nagli. ‘‘UV Gated Raman Spectroscopy for Standoff Detection of Explosives.’’ Opt. Mater. 2008. 30(11): 1739–1746.
28. J. Moros, J.A. Lorenzo, K. Novotny´, J.J. Laserna. ‘‘Fundamentals of Stand-off Raman Scattering Spectroscopy for Explosive Fingerprinting.’’ J. Raman Spectrosc. 2013. 44(1): 121–130.
29. A. Pettersson, S. Wallin, H. Ostmark, A. Ehlerding, I.Johansson, M. Nordberg, H. Ellis, A. Al-Khalili. ‘‘Explosives Standoff Detection using Raman Spectroscopy: from Bulk Towards Trace Detection.’’ Proc. SCIE. 2010.76641K: 1–12.
30. J.C. Carter, J. Scaffidi, S. Burnett, B. Vasser, S.K. Sharma, S.M. Angel. ‘‘Stand-off Raman Detection using Dispersive and Tunable Filter Based Systems.’’ Spectrochim. Acta, Part A. 2005. 61(10): 2288–2298.
31. J.C. Carter, S.M. Angel, M. Lawrence-Snyder, J. Scaffidi, R.E. Whipple, J.G. Reynolds. ‘‘Standoff Detection of High Explosive Materials at 50 Meters in Ambient Light Conditions Using a Small Raman Instrument.’’ Appl. Spectrosc. 2005. 59(6): 769–775.

32. M. Wu, M. Ray, K.H. Fung, M.W. Ruckman, D. Harder, A.J. Sedlacek. ‘‘Stand-off Detection of Chemicals by UV Raman Spectroscopy.’’ Appl. Spectrosc. 2000. 54(6): 800–806.

33. M.D. Ray, A.J. Sedlacek, M. Wu. ‘‘Ultraviolet Mini-Raman Lidar for Stand-off, In Situ Identification of Chemical Surface Contaminants.’’ Rev. Sci. Instrum. 2000. 71(9): 3485–3489.

34. M. Skulinova, C. Lefebvre, P. Sobron, E. Eshelman, M. Daly, J.-F. Gravel, J.F. Cormier, F. Chaˆteauneuf, G. Slater, W. Zheng, A. Koujelev, R. Leveille. ‘‘Time-resolved Stand-off UV-Raman Spectroscopy for Planetary Exploration.’’ Planet. Space Sci. 2014. 92: 88–100.

35. T.J. Kulp, S.E. Bisson, T.A. Reichardt. ‘‘Standoff Ultraviolet Raman Scattering Detection of Trace Levels of Explosives.’’ Sandia Natl. Lab. [Tech. Rep.] Sandia Report. 2011. 7955. doi:10.2172/1030305.

36. R.L. McCreery. ‘‘Magnitude of Raman Scattering.’’ In: T.D. Winefordner (ed.) Raman Spectroscopy for Chemical Analysis. New York, NY: John Wiley & Sons, Inc, 2000, pp.15–33.

37. S.A. Asher. ‘‘UV Resonance Raman Spectroscopy for Analytical, Physical, and Biophysical Chemistry. Part 1.’’ Anal. Chem. 1993. 65(2): 59A–66A.

38. M. Ghosh, L. Wang, S.A. Asher. ‘‘Deep-Ultraviolet Resonance Raman Excitation Profiles of NH_4NO_3, PETN, TNT, HMX, and RDX.’’ Appl. Spectrosc. 2012. 66(9): 1013–1021.

39. S.A. Asher, C.R. Johnson. ‘‘Raman Spectroscopy of a Coal Liquid Shows that Fluorescence Interference is Minimized with Ultraviolet Excitation.’’ Science. 1984. 225(4659): 311–313.

40. N. Lamsal, S.M. Angel. ‘‘Deep-Ultraviolet Raman Measurements Using a Spatial Heterodyne Raman Spectrometer (SHRS).’’ Appl. Spectrosc. 2015. 69(5): 525–534.

41. N. Lamsal, S.M. Angel, S.K. Sharma, T.E. Acosta. ‘‘Visible and UV Standoff Raman Measurements in Ambient Light Conditions Using a Gated Spatial Heterodyne Raman Spectrometer.’’ Paper presented at: LPSC 2015. Woodland, TX; March 16–20 2015.

42. N. Lamsal, S. K. Sharma, T. E. Acosta, S. M. Angel. “Ultraviolet Stand-off Raman Measurements Using a Gated Spatial Heterodyne Raman Spectrometer.” Appl. Spectrosc., in press 2016, DOI: 10.1177/0003702816631304.

43. G. Hu, W. Xiong, H. Shi, Z. Li, J. Shen, X. Fang. “Raman Spectroscopic Detection for Liquid and Solid Targets using a Spatial Heterodyne Spectrometer.” J. Raman Spectrosc. 2016. 47(3): 289-298.

44. G. Hu, W. Xiong, H. Shi, Z. Li, J. Shen, X. Fang. “Raman Spectroscopic Detection using Two-Dimensional Spatial Heterodyne Spectrometer.” Opt. Eng. 2015. 54(11): 114101-1 - 114101-9.

45. P. D. Barnett, N. Lamsal, S. M. Angel. “Standoff LIBS using a Miniature Wide Field of View Spatial Heterodyne Spectrometer with Sub-Microsteradian Collection Optics.” Appl. Spectrosc. Submitted for publication February 2016.

46. P. Matousek, A.W. Parker. “Bulk Raman Analysis of Pharmaceutical Tablets.” Appl. Spectrosc. 2006. 60(12): 1353-1357.2

47. J. Johansson, A. Sparen, O. Svensson, S. Folestad, M. Claybourn. “ Quantitative Transmission Raman Spectroscopy of Pharmaceutical Tablets and Capsules.” Appl. Spectrosc. 2007. 61(11): 1211-1218.

48. N. Stone, P. Matousek. “Advanced Transmission Raman Spectroscopy: A Promising Tool for Breast Disease Diagnosis.” Cancer Res. 2008. 68(11): 4424-4430.

49. C. Eliasson, N.A. Macleod, L.C. Jayes, F.C. Clarke, S.V. Hammond, M.R. Smith, P. Matousek. “Non-invasive Quantitative Assessment of the Content of Pharmaceutical Capsules Using Transmission Raman Spectroscopy.” J. Pharm. Biomed. Anal. 2008. 47(2): 221-229.

50. N.A. Macleod, P. Matousek. “Emerging Non-invasive Raman Methods in Process Control and Forensic Applications.” Pharmaceut. Res. 2008. 25(1): 2205-2215.

51. N. Everall, T. Hahn, P. Matousek, A. W. Parker, M. Towrie. “Picosecond Time-Resolved Raman Spectroscopy of Solids: Capabilities and Limitations for Fluorescence Rejection and the Influence of Diffuse Reflectance.” Appl. Spectrosc. 2001. 55(12): 1701–1708.

52. N. Everall, P. Matousek, N. MacLeod, K.L Ronayne, I.P. Clark. “Temporal and Spatial Resolution in Transmission Raman Spectroscopy.” Appl. Spectrosc. 2010. 64(1): 52-60.

53. N. Everall, I. Priestnall, P. Dallin, J. Andrews, I. Lewis, K. Davis, H. Owen, M.W. George. “Measurement of Spatial Resolution and Sensitivity in

Transmission and Backscattering Raman Spectroscopy of Opaque Samples: Impact on Pharmaceutical Quality Control and Raman Tomography." Appl. Spectrosc. 2010. 64(5): 476-484.

54. D. Oelkrug, E. Ostertag, R.W. Kessler. "Quantitative Raman Spectroscopy in Turbid Matter: Reflection or Transmission Mode?" Anal. Bioanal. Chem. 2013. 405(10): 3367-3379.
55. M.J. Pelletier, P. Larkin, M. Santangelo. "Transmission Fourier Transform Raman Spectroscopy of Pharmaceutical Tablet Core." Appl. Spectrosc. 2012. 66(4): 451-457.
56. M.J. Pelletier. "Sensitivity-Enhanced Transmission Raman Spectroscopy." Appl. Spectrosc. 2013. 67(8): 829-840.
57. P. Matousek. "Raman Signal Enhancement in Deep Spectroscopy of Turbid Media." Appl. Spectrosc. 2007. 61(8): 845-854.
58. K. Shin, H. Chung. " Wide Area Coverage Raman Spectroscopy for Reliable Quantitative Analysis and its Applications." Analyst 2013. 138(12): 3335-3346.

CHAPTER 2

CHARACTERIZATION OF A VISIBLE SPATIAL HETERODYNE RAMAN SPECTROMETER (SHRS) FOR STANDOFF DETECTION

2.1 Abstract

A visible spatial heterodyne Raman spectrometer (SHRS) was demonstrated and characterized for standoff detection at 4.5 meters. With this system, the field-of-view of the SHRS was demonstrated to be ~1.8 - 2° corresponding to a spot size of ~74 - 80 mm for a sample 4.5 m from the collection optics. Off-axis sample excitation was demonstrated to be acceptable up to ~4 cm from the optical axis at 4.5 m, which relaxes the laser pointing and sample position accuracy requirements for standoff Raman. 1D standoff Raman imaging was also demonstrated using a cylindrical lens at the input of the SHRS to spatially resolve a vertically layered sample on the CCD. The spectral resolution of the imaged spectra in comparison to the non-imaging spectra for the same sample remained the same, while the signal-to-noise ratio improved, with up to four times higher SNR for particular bands. The spatial resolution was 280 mm at 4.5 m.

2.2 Indroduction

Raman spectroscopy is an inelastic scattering technique used to probe the vibrational modes of a molecule, providing detailed information about the molecular structure of the sample and a molecular “fingerptint”. As a scattering technique, Raman spectroscopy offers analysis without sample preparation and has been demonstrated as a valuable technique for analyzing organic and inorganic samples in bench-top and standoff configurations.[1-2] Raman spectroscopy is easily amenable to standoff detection as long as the sample is within the line of sight of the collection optics, and standoff Raman spectroscopy enables detection of inaccessible samples.

A typical standoff Raman experiment is performed by using a laser to illuminate a sample at a distance of tens to hundreds of meters, and the Raman scattered light is collected by a telescope and directed into a spectrometer. Standoff Raman was first described and demonstrated for atmospheric gas measurements,[3-6] and was later extended to measurements of inorganic and organic compounds using a portable Raman standoff system developed for radioactive wastes analysis in underground storage tanks.[7] Other recent advances in standoff Raman spectroscopy include: remote measurements up to 1500 m[8]; systems designed for planetary exploration[9-11] and explosives detection[12-14]; gated detection for ambient light operations[15-16]; and systems developed to take advantage of the resonance enhancement and higher Raman cross sections in the deep-UV.[12,17-23] Excitation at deep-UV wavelengths has been shown to provide Raman spectra free from interference of longer wavelength fluorescence, which often plagues visible wavelength Raman measurements.[24] However, UV excited standoff Raman measurements require a high resolution spectrometer capable of resolving the closely spaced Raman bands observed in a narrow spectral range, and care must be taken to avoid laser-induced photodegradation by utilizing low laser irradiance. Spectrometers with sufficiently high spectral resolution for deep-UV Raman typically require large, high dispersion gratings and long focal length optics, making the spectrometer large with low light throughput. Therefore, conventional dispersive spectrometers will lose sensitivity when using wide area laser beams to reduce sample irradiance, and due to the large size, high resolution dispersive spectrometers are not ideal as portable instruments.

The spatial heterodyne Raman spectrometer (SHRS) is a compact, high resolution instrument first described by Gomer et al. for visible Raman measurements,[25] and later

extended for deep UV[26-27] and standoff UV Raman measurements.[28] The SHRS is based on a dispersive interferometer, similar in design to a Michelson interferometer with the mirrors replaced by stationary diffraction gratings. The SHRS has no moving parts and all wavelengths are measured simultaneously, which makes the system compatible with pulsed lasers and gated detection. The SHRS does not require an entrance slit to maintain high resolution and has a large angular field of view (FOV), making the optical Etendue of the system profoundly larger than that of a conventional dispersive spectrometer. The large Etendue of the SHRS allows wide area measurements to be made without losing sensitivity or spectral resolution and sample photodegradation can be avoided by using large laser spots on the sample. For standoff Raman measurements, the large entrance aperture of the SHRS should reduce telescope alignment constraints and minimize laser pointing stability issues, because small movements of the laser spot on the target do not reduce the amount of light collected by the spectrometer, as recently demonstrated in our lab for standoff LIBS measurements.[29] There are no published quantitative studies to measure the field-of-view (FOV) of the SHRS for standoff Raman, or the laser irradiance and associated beam size necessary to reduce photodegradation. The work presented quantifies the FOV (i.e. width of the area viewed) and beam diameter and laser irradiance required to reduce photodegradation of sulfur, and also demonstrates 1D imaging using wide area illumination.

2.3 Experimental

2.3.1 SHRS

Figure 2.1 shows a schematic of the SHRS. The basic instrument design was previously described.[25-28] The SHRS design used for this work consisted of a 25 mm cube beam splitter (CM1-BS013, ThorLabs) and two 25 mm, 150 grooves/mm diffraction gratings blazed at 500 nm. A grating mount (DGM-1; Newport Corp.) was used to manually control the grating rotation angle to precisely set the Littrow wavelength. A 105 mm focal length, f/2.8 lens (AF Micro-Nikkor; Nikon) was used to image the gratings at unity magnification onto a liquid nitrogen cooled charge-coupled device (CCD) detector with 1340 X 1300, 20 micron pixels (VersArray; Princeton Instruments). The fringe pattern was recorded on the CCD using Winspec (32-bit, version 2.5.22.0), and data processing was performed using Matlab (MathWorks, version R2013a) and IGOR Pro (WaveMetrics, version 6.03A2) software.

A 532 nm diode-pumped continuous wave (CW) laser (Millennia Pro 2s; Spectra-Physics) was used as the excitation source for all spectra presented, and was also used to set the Littrow angle of the gratings to 532 nm. Raman light was collected from the remote sample using a 60 mm diameter, 490 mm focal length achromatic lens (L_1), collimated to a 25 mm beam using an achromatic, 250 mm focal length, 50.8 mm diameter, MgF_2 coated lens (PAC088; Newport Corp.)(L_2) and directed into the SHRS. For 1D imaging, L_2 was replaced by a 200 mm focal length, 25.4 mm diameter achromatic lens (lens info), and an additional 400 mm focal length, 30 mm high plano convex cylindrical lens (lens info) was placed in the collimated input beam. The collimated light was filtered using various combinations of three filters: a 600 nm short-

pass filter (10SWF-600-B; Newport Corp.) to block out-of-band light, and a 532 nm long-pass filter (LP03-532RE-25; Semrock) and 532 nm holographic filter (Supernotch; Kaiser Optical Systems Inc.) for laser line rejection. Filters limited the aperture to 22.8 mm.

2.3.2 Samples

Sulfur, potassium perchlorate, sodium nitrate, sodium nitrite, sodium sulfate, and ammonium nitrate were purchased from Sigma-Aldrich at 99%+ purity and used "as is." Potassium nitrate, 99+%, was purchased from Mallinckrodt Chemical. Calcite, α-quartz, gypsum, and olivine were natural rock and mineral samples.

2.4 Results and Discussion

2.4.1 SHRS

The SHRS is based on a dispersive interferometer, similar to a Michelson interferometer with stationary gratings used in the place of moving mirrors, see Figure 2.1. The Raman signal from the sample is collimated and directed into the interferometer, split into two beams, and directed to the gratings in each arm of the interferometer. The gratings are tilted to a specific angle, the Littrow angle θ_L, so that at the Littrow wavelength the light is exactly retro-reflected. All other wavelengths are heterodyned to the Littrow wavelength and form an interference pattern. The interference pattern is imaged onto a CCD to produce a fringe image.[25-28] The fringe pattern is summed in the vertical direction into a fringe cross section and taking the Fourier transform of the fringe pattern cross section recovers the Raman spectrum. The number of fringes observed is defined by:

$$f = 4(\sigma - \sigma_L)\tan\theta_L \qquad \text{Equation 2.1}$$

where f is fringes per centimeter, σ is the wavenumber of the Raman band, and σ_L is the Littrow wavenumber. The intensity of the fringe pattern is a function of position x, given by:

$$I(x) = \int_0^\infty B(\sigma)\{1 + \cos[8\pi(\sigma - \sigma_L)x\tan\theta_L]\}d\sigma \qquad \text{Equation 2.2}$$

where $B(\sigma)$ is the input spectral intensity, and the Fourier transform of $I(x)$ yields the Raman spectrum.[30-33]

Unlike a dispersive spectrometer, the SHRS entrance aperture does not strongly affect the resolution of the spectrometer. So large apertures can be used giving very high throughput with high spectral resolution without loss of spectral resolution. The resolving power (R) of the SHRS is equal to the number of grooves illuminated on the gratings, about 6800 for the system used here, giving a 2.6 cm^{-1} theoretical spectral resolution.[30] The spectral resolution of the SHRS was measured using a low pressure Hg lamp to be ~8 cm^{-1}. Factors that affect the resolution include camera focusing, collimation of the input beam, and the quality of the gratings and imaging optics. The spectrometer throughput, or Etendue, is the product of the area viewed and the collection solid angle. The collection solid angle of the SHRS, Ω_S, is defined in Equation 3.[30]

$$\Omega_S = 2\pi/R \qquad \text{Equation 2.3}$$

For the system used here, the collection solid angle is about 9.2 x 10^{-4} sr, giving an acceptance angle of ~3 x 10^{-2} radians (i.e. 1.7°). The width of the area viewed for standoff Raman is the product of the instrument acceptance angle, α, and the distance, d, to the

sample. Therefore, the calculated width of the area viewed with the optical set up described here and for a sample at a distance of 4.5 is ~66 mm.

2.4.2 Representative Raman spectra

One of the primary motivations for developing the SHRS is for planetary exploration. Figure 2.2 shows Raman spectra of some types of samples that might be relevant for Mars exploration (i.e. minerals, rocks, water, and ice).[11] The Raman spectra of calcite, α-quartz, olivine, and gypsum were measured using the SHRS with the sample at a distance of 4.5 meters using the 60 mm collection lens. The measured spectral resolution for the sample Raman bands ranged from 8.8 to 16.4 cm^{-1}; a little larger than the measured resolution of the instrument. The measured spectra match well to Raman spectra reported for similar samples in the literature. The symmetric breathing vibration of carbonate at 1086 cm^{-1} is most prominent Raman band in the calcite spectrum.[34] The Raman spectrum of quartz displayed the silica symmetric vibrational modes at 210, 357, and 468 cm^{-1} characteristic of low temperature phase α-quartz.[35] Olivines are silicate-based minerals, and the silicate Raman bands present in the spectrum are the stretching combinations at 821 and 854 cm^{-1}, the anti-symmetric stretches at 919 and 960 cm^{-1}.[36] The gypsum ($CaSO_4 \cdot 2H_2O$) Raman spectrum has six characteristic Raman bands of the sulfate ion: the symmetric stretch at 1008 cm^{-1}, anti-symmetric bending at 412 and 495 cm^{-1}, anti-symmetric stretch at 1135 cm^{-1}, and anti-symmetric bending at 613 and 672 cm^{-1}.[37]

All four spectra show some degree of luminescence from impurities, and no spectral background subtraction was used to remove this. Signal-to-noise ratios in the

Raman spectra are 85, 325, 38, and 179 for the strongest bands shown of the calcite, α-quartz, olivine, and gypsum samples, respectively. The interferogram for each sample is shown as an inset in Figure 2.2. The quality of the interferogram is given by the fringe visibility (FV), which is defined by Equation 4. The FV for the samples shown was 0.11, 0.17, 0.26, and 0.23 for the calcite, α-quartz, olivine, and gypsum samples, respectively. The FV was mainly limited, for the SHRS described, by high levels of stray light.

$$FV = (I_{max}-I_{min})/(I_{max}+I_{min}) \qquad \text{Equation 2.4}$$

Figure 2.3 shows the Raman spectra of a 2.2 x 10^{-3} M sodium sulfate solution measured with the SHRS as a room temperature liquid (lower) and frozen at ~77 K (middle), as well as solid sodium sulfate (top). The ice sample was frozen and kept cold using liquid nitrogen, and both the ice and water solutions were 70 mm thick. All Raman bands present in the spectra are internal vibrations of the sulfate ion,[37-39] and there are clear differences in the number of Raman bands present, the exact wavenumber position, and resolution. The spectral resolution for the sulfate Raman band was ~10 cm^{-1} for the solid and frozen solution and 12.6 cm^{-1} for the liquid solution. The observed broadening and downshift in the Raman bands, 992, 973, and 980 cm^{-1} for the solid, frozen solution, and liquid solution, respectively, is consistent with increasing hydration.[38] The differences observed in the spectra can be used to discriminate different phases, forms, and temperature of a sample,[38-42] which makes Raman spectroscopy a useful technique for planetary exploration.

2.4.3 Width of area viewed and off-axis detection at 4.5 meters

The wide acceptance angle of the SHRS allows wide area measurements to be made without losing sensitivity or spectral resolution, unlike a slit-based dispersive spectrometer that requires all light to enter through a narrow slit to maintain high spectral resolution. Although measurements with large laser beam diameters have been demonstrated using an SHRS,[25, 27-28] the laser spot sizes were never close to limit of the width of area viewed by the SHRS. Therefore, measurements were made at the limit of the theoretical width of the area viewed, ~66 mm with current optical set up at 4.5 m.

Figure 2.4 demonstrates the width of the area viewed by the SHRS using a solid 10 cm diameter sulfur sample located 4.5 m from the collection optics. Raman spectra were measured as the size of the laser spot on the sample was varied from ~200 um to ~50 mm. The inset shows a Raman spectrum for each beam size measured. The size of the laser spot on the sample was measured using a razor edge to block the beam as the power was measured. The diameter of the beam was taken as the distance between the 5% and 95% values in the fitted curve. In Figure 2.4, the intensity of the sulfur 219 cm^{-1} Raman band is plotted against the measured beam diameter to determine the width of the area viewed by the SHRS.

The plot shows a slight decrease in intensity as the beam diameter is increased, as expected with any spectrometer measuring off-axis light. The beam expander used limited the largest beam size to ~50 mm, so the width of area viewed could not be fully tested by expanding the beam up to and beyond the theoretical width of area viewed. However, the data shows the width of the area viewed by the current optical set up is at

least ~50 mm without a loss in Raman signal, and to test the limits of the width of the area viewed, another method was used.

In Figure 2.4, the spectra do not show any band broadening as the laser spot size is increased up to ~50 mm, which demonstrates the capability of the SHRS to measure large diameter beams with no loss in spectral resolution. Some spectra show a one pixel shift in the maximum Raman band intensity, but the occurrence seems to be random and not related to the laser spot size.

Another way to test the width of area viewed by the SHRS is to measure the Raman signal as the laser spot is moved off the optical axis. The measured quantity in this experiment is the radius of the width of the area viewed; therefore, the result must be doubled to determine the full width of the area viewed. Figure 2.5 demonstrates the width of the area viewed, as well as the off-axis capability of the SHRS for a $KClO_4$ powder sample at a distance of 4.5 m, with a laser spot size of ~2 mm. The sample and laser were positioned on the optical axis, and moved in 0.5 cm increments in the horizontal direction. The experiment was also performed, by using a 10 cm diameter Na_2SO_4 sample and only moving the laser away from the optical axis in 0.6 cm increments, to verify the results. Note: During the off-axis experiment using the Na_2SO_4 sample, a 9 mm aperture was used as a spatial filter, see Figure 2.1.

Figure 2.5 shows the average baseline-subtracted intensity of the 942 cm^{-1} Raman band for $KClO_4$ (left axis) versus the distance of the sample and laser from the optical axis, as well as the 992 cm^{-1} Raman band for Na_2SO_4 (right axis) versus the distance of the laser from the optical axis. The Raman spectra of the Na_2SO_4 and $KClO_4$ are inset in

Figure 2.5. The distance at which the Raman intensity drops to 1/e of the maximum intensity for the Na_2SO_4 and $KClO_4$ is ~37 and 40 mm, respectively, from the optical axis, which corresponds to a ~74 - 80 mm width of area viewed and an angular FOV of ~1.8 - 2°. Although the amount of tailing is lower for the Na_2SO_4 curve due to the spatial filter in place, the experimental results were the same for both experiments.

There is a slight intensity increase around 1 cm in Figure 2.5, which is consistent with results obtained using spatially resolved spectroscopy for highly scattering samples as described by Oelkrug, et al.[43-44] Diffuse laser and Raman scattering in the sample generates Raman photons over a larger area than that illuminated by the excitation laser, which increases the sampling area. The diffuse scattering can lead to stronger Raman signals coming from a sample region slightly shifted from the point where the sample is illuminated by the laser.[42-43] As the laser moves further from the optical axis, the signal begins to decrease even though the width of the area viewed limit has yet to be reached, because the diffusely scattered Raman begins to move outside the collection area of the SHRS. Off-axis detection increases the tolerance in laser pointing stability and accuracy, as well as makes aligning the optical axis of the spectrometer precisely on the sample much more

2.4.4 *Reducing photodegradation using large laser spot sizes to reduce irradiance*

As demonstrated above, the SHRS offers the unique capability of measuring samples with wide area illumination without loss of sensitivity or spectral resolution. Using larger laser spots on the sample leads to reduced laser irradiance without a loss in laser power or Raman signal, which can be used to avoid photodegradation. Using larger

beams to reduce photodegradation has been demonstrated previously using the SHRS.[25-28] However, the previous studies did not quantify the beam size or irradiance necessary to reduce photodegradation.

Figure 2.6 shows a plot of the 219 cm^{-1} sulfur Raman band intensity as a function of laser power, using different laser spot sizes, and thus different sample irradiance (the curves are offset for clarity). The laser irradiance on the sample for the 0.25, 3, 19, and 64 mm beam was 240-2400, 1.7-17, 0.043-0.42, and 0.0037-0.037 W/cm^2, respectively. The sample was moved between each measurement for the 250 mm and 3 mm beams. At the larger beam sizes, the Raman intensity increases in proportion to the laser power increase, indicating there is no sample degradation. Whereas, the smaller spot size curves are nonlinear indicating sample degradation. The results confirm that as the beam diameter is increased, the laser irradiance on the sample decreases, reducing sample photodegradation and suggests an irradiance of ~0.42 W/cm^2 or less as to avoid photodegradation for sulfur. The wide FOV makes the SHRS uniquely suited to this type of measurement.

2.4.5 1D Imaging using a SHRS

Raman imaging is a powerful technique to look for heterogeneities in a sample or to look at mixed samples. For example, the spatial distribution of the heterogeneities in a geological sample can provide information about how the geological samples were formed.[45] The SHRS is well suited to Raman imaging, and Smith, et al described several approaches to imaging with the SHS.[46] For 1D SHRS imaging, a cylindrical lens is added to the collection optics to focus an image of the sample onto the gratings in the vertical

direction. In the SHRS, the gratings, along with the sample image are imaged onto the CCD. The optical set up is similar to that in Figure 2.1, except L_2 was replaced by a 200 mm focal length, 25.4 mm diameter achromatic lens, and a 400 mm focal length, 30 mm high cylindrical lens was placed between the L_2 and the grating to image the scene onto the grating.

To test 1D Raman imaging with the SHRS, a mixed sample was constructed by vertically stacking three 1 cm cuvettes containing $KClO_4$, NH_4NO_3, and a $NaNO_3/NaNO_2$ mixture. The samples were all simultaneously illuminated using a 3.5 - 4.0 cm laser spot. Figure 2.7 (inset) shows Raman images of the sample without the use of the cylindrical imaging lens (lower inset), and a 1D image using the cylindrical imaging lens (upper inset). The collimated Raman spectrum (lower) clearly shows all four components with good resolution. The top three Raman spectra show the resolved individual components, where each spectrum was extracted from the top, middle, and lower portions of the 1D Raman image by vertically binning the rows corresponding to the three cuvettes. Rows one, two, and three in Figure 2.7 are the spectra of $KClO_4$, NH_4NO_3, and the $NaNO_3/NaNO_2$ mixture, respectively. The collimated input beam spectrum is a combination of all four components, since the Raman information is not spatially resolved in any direction. The spectral resolution, ~8 - 13 cm^{-1}, was the same for both types of measurements. Spectral resolution is directly proportional to the number of grating grooves illuminated, and the same number of grooves is illuminated using either the collimated beam or the cylindrical lens. More importantly, the signal-to-noise ratio (SNR) of the Raman spectra obtained using the 1D Raman image is up to four times higher than without imaging, for the major Raman bands. SNR for the collimated beam

input spectra were 104, 289, 129, and 12 for the 942, 1043, 1068, and 1325 Raman bands of $KClO_4$, NH_4NO_3, and the $NaNO_3/NaNO_2$ mixture, respectively, and the SNR for the imaged spectra were 402, 463, 415, and 30 for the 942, 1043, 1068, and 1325 Raman bands of $KClO_4$, NH_4NO_3, and the $NaNO_3/NaNO_2$ mixture, respectively. SNR improvement is attributed to the decreased number of Raman bands present in each spectrum obtained from the 1D Raman image, because in an interferometer, noise in all bands is distributed equally across the spectrum.[29]

The 1D imaging spatial resolution was also determined by measuring a sample using wires of known thicknesses positioned on top of the sample, and the thinnest wire observable in the image was taken as the spatial resolution. The spatial resolution measured for the 1D images of samples at a distance of 4.5 m was ~280 μm; lower spatial resolution may be necessary to spatially resolve heterogeneities in geological samples[45] and can be achieved by using a CCD with smaller pixels, or by changing the magnification of the imaging or collection optics.

2.6 Conclusion

A spatial heterodyne Raman spectrometer has been used to measure rock samples, as well as liquid and 77 K frozen solutions, at distance of 4.5 meters. The width of the area viewed by the SHRS at this distance was found to be ~74 - 80 mm, corresponding to a FOV of 1.8 - 2.0°. The wide area measurement capability of the SHRS was used to demonstrate decreased sample photodegradation by using very large laser spots on the sample, without loss of signal or decreased spectral resolution. 1D Raman imaging using the SHRS was demonstrated and shown to provide better signal-to-noise ratio spectra

than spectra measured without imaging. Improved SNR using 1D imaging is the result of spatial separation of the signal from different samples, which reduces the contribution of noise from adjacent samples. The spatial resolution of the SHRS when used for 1D imaging at 4.5 m was ~280 μm.

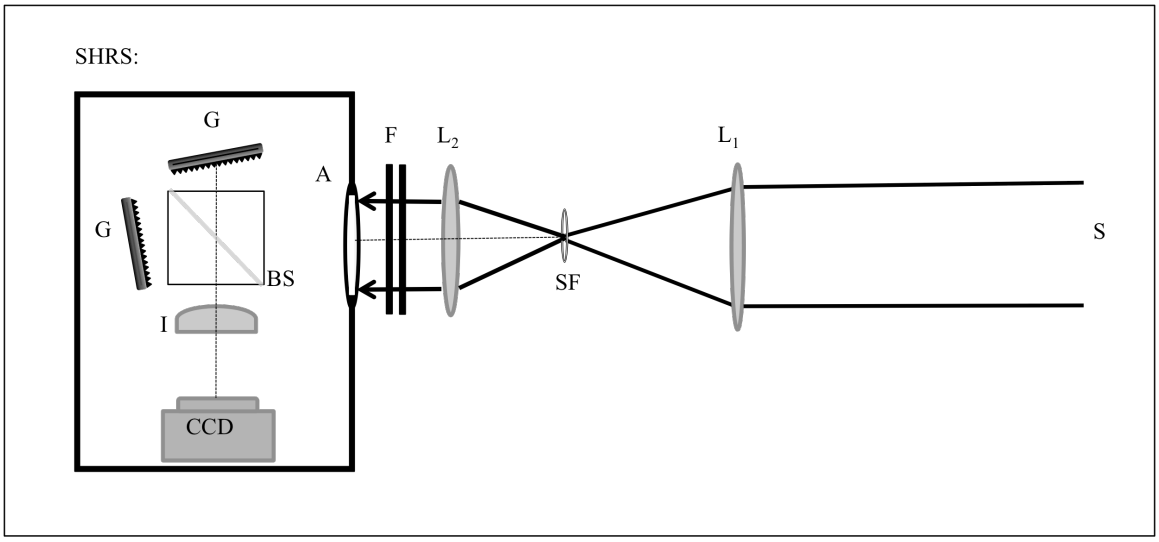

Figure 2.1: SHRS schematic- The Raman light collected by L_1 is focused down and re-collimated by L_2 and directed into the entrance aperture (A.). The light is split 50/50 by the beam splitter (BS). The gratings (G) disperse the light back towards the beam splitter, where the wavefronts recombine. The imaging lens (I) images the gratings onto the CCD detector. SF is a spatial filter, variable in size, used in some of the experiments.

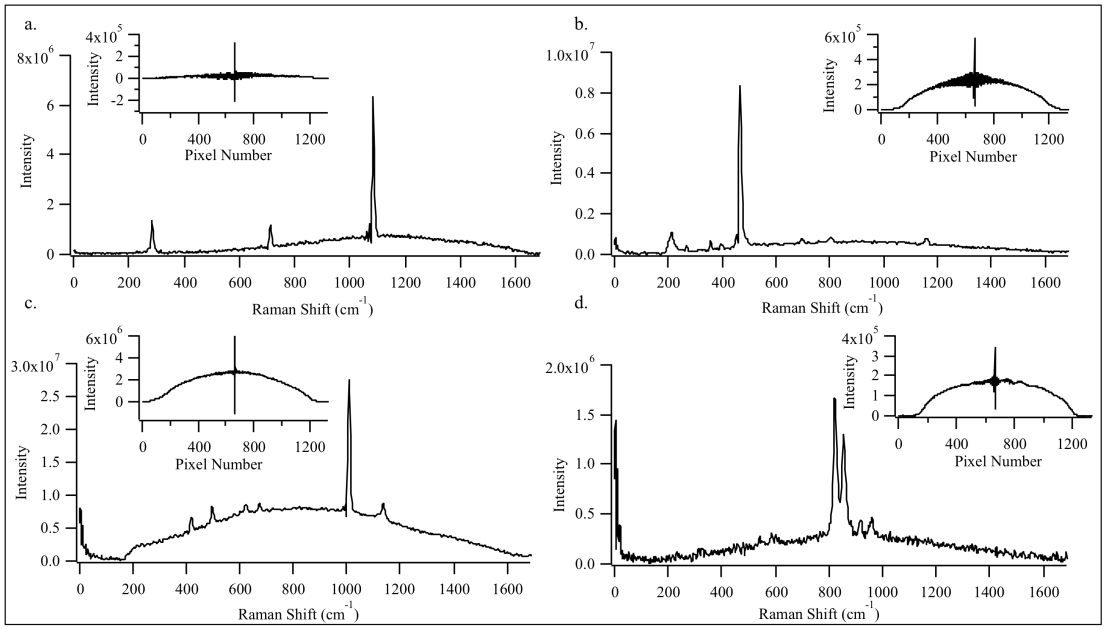

Figure 2.2: Raman spectra and corresponding fringe cross sections of rock samples measured with the SHRS using a 2 W, 532 nm laser at 4.5 m. The top two spectra, calcite (a.) and quartz (b.), were measured for 30 sec. acquisition time. The lower two spectra, gypsum (c.) and olivine (d.), were measured for 60 sec. and 90 sec. acquisition time, respectively.

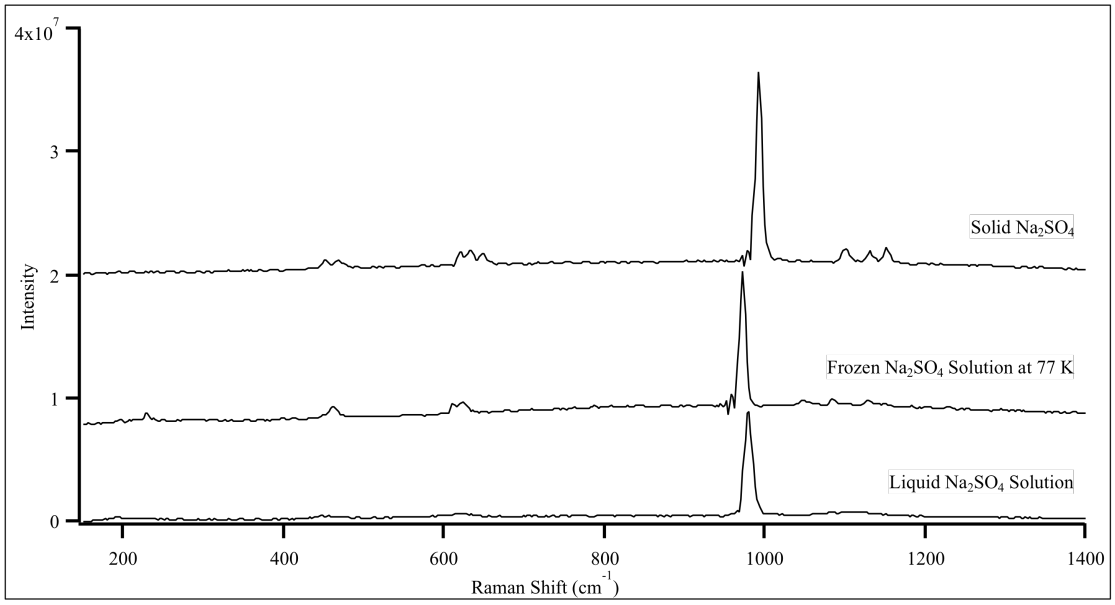

Figure 2.3: Raman spectra of solid sodium sulfate (top) and a 2.2 x 10^{-3} M sodium sulfate solution measured with the SHRS as a liquid (lower) and frozen at 77 K (middle), offset for clarity. Spectra measured for 90 and 30 second acquisition times for the solutions and solid, respectively, using 532 nm laser at ~2 W power.

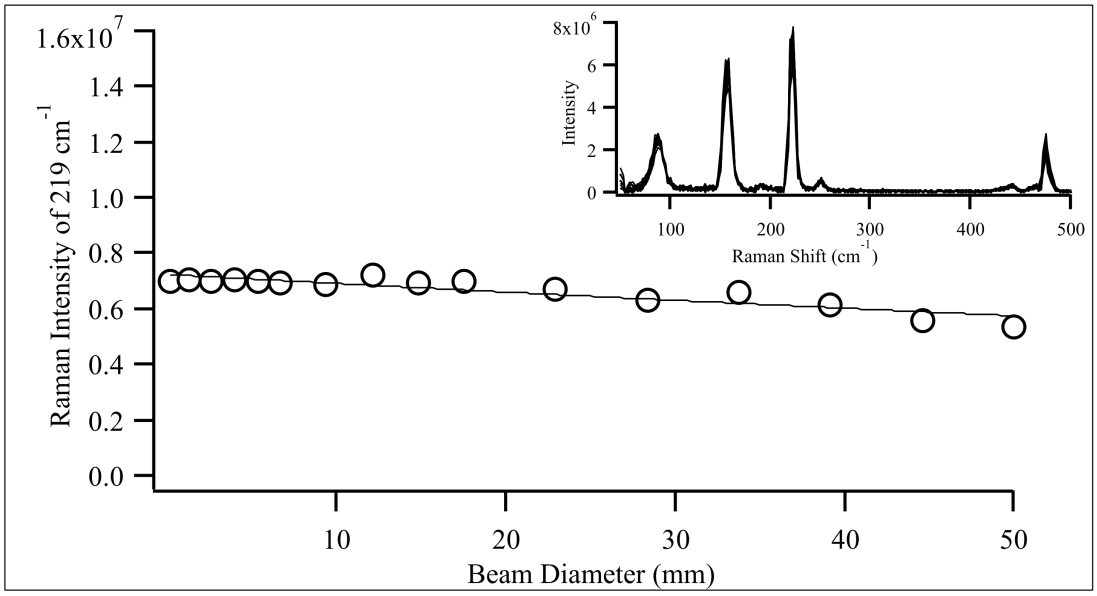

Figure 2.4: Plot of Raman intensity of the 219 cm^{-1} sulfur band as beam diameter is increased from ~200 mm to ~50 mm. The Raman spectra were measured with a 532 nm laser at 200 mW for a 10 sec. acquisition time. The upper right inset are the Raman spectra of sulfur, one spectrum for each beam size measured.

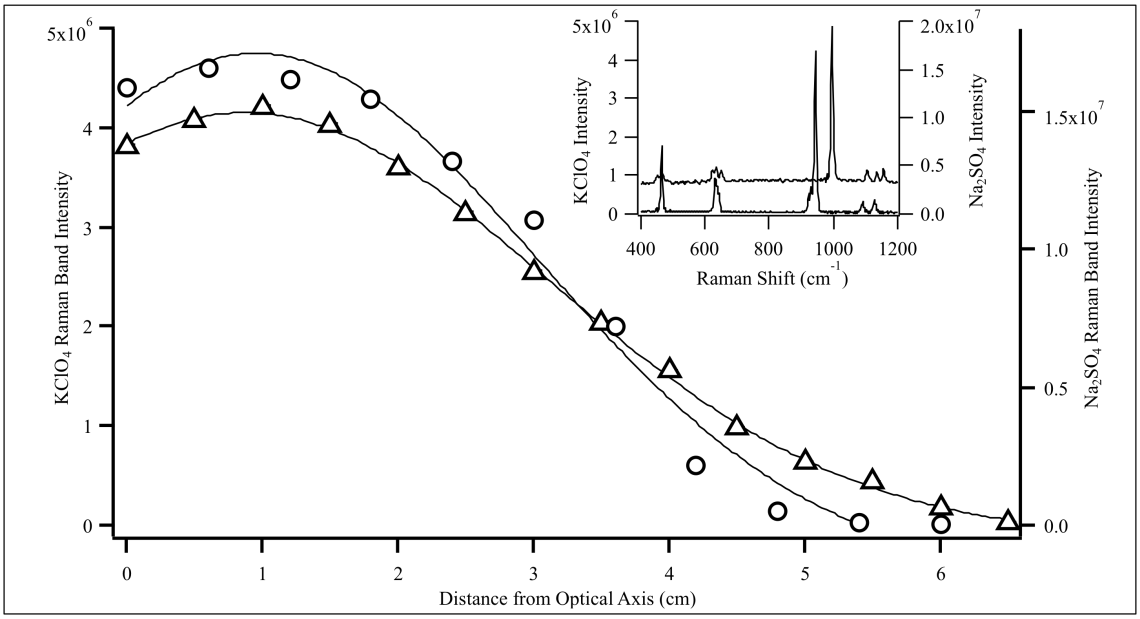

Figure 2.5: Plot of the Raman intensity of potassium perchlorate (triangles, left axis) and sodium sulfate (circles, right axis) as the laser is moved away from optical axis. Inset is Raman spectra of potassium perchlorate (lower) and sodium sulfate (top), offset for clarity. Raman spectra of potassium perchlorate in a 1 cm cuvette were measured using a 532 nm laser at ~700 mW for 15 sec. acquisition time. Raman spectra of a 10 cm diameter sodium sulfate sample were measured using a 532 nm laser at ~1.5 W for 30 sec. acquisition time.

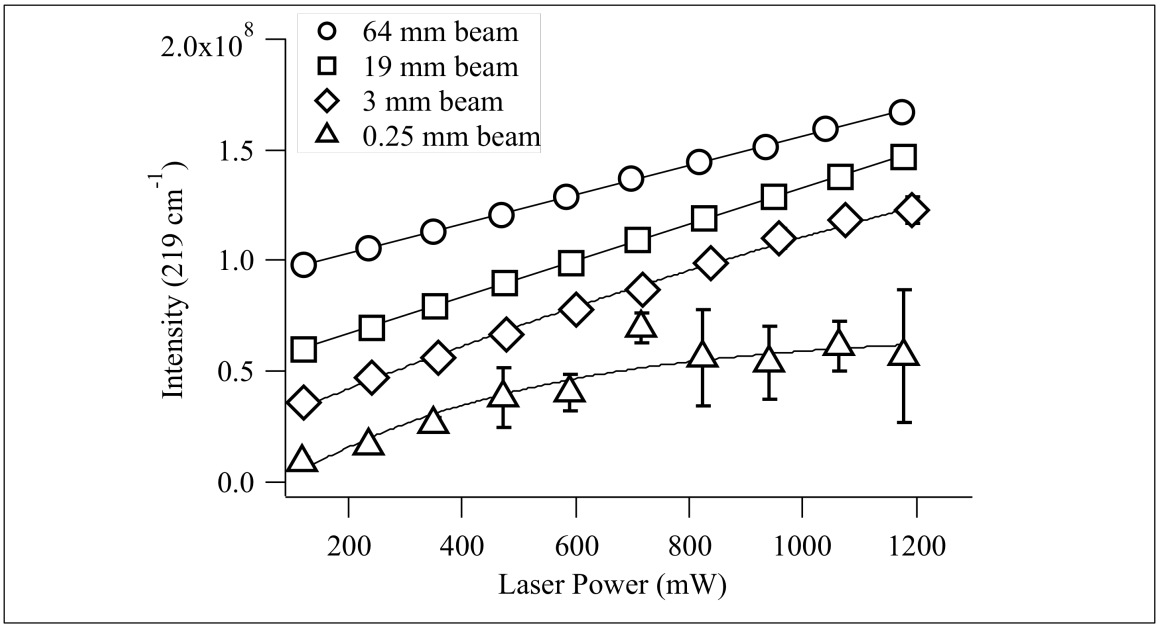

Figure 2.6: Plot of the Raman intensity of the 219 cm^{-1} sulfur band as laser power is varied using various laser beam diameters. The 0.25 (triangle) and 3 (diamond) mm beams presented signs of photodegradation, but the 19 (square) and 64 (circle) mm beams were free of photodegradation. Plots offset for clarity.

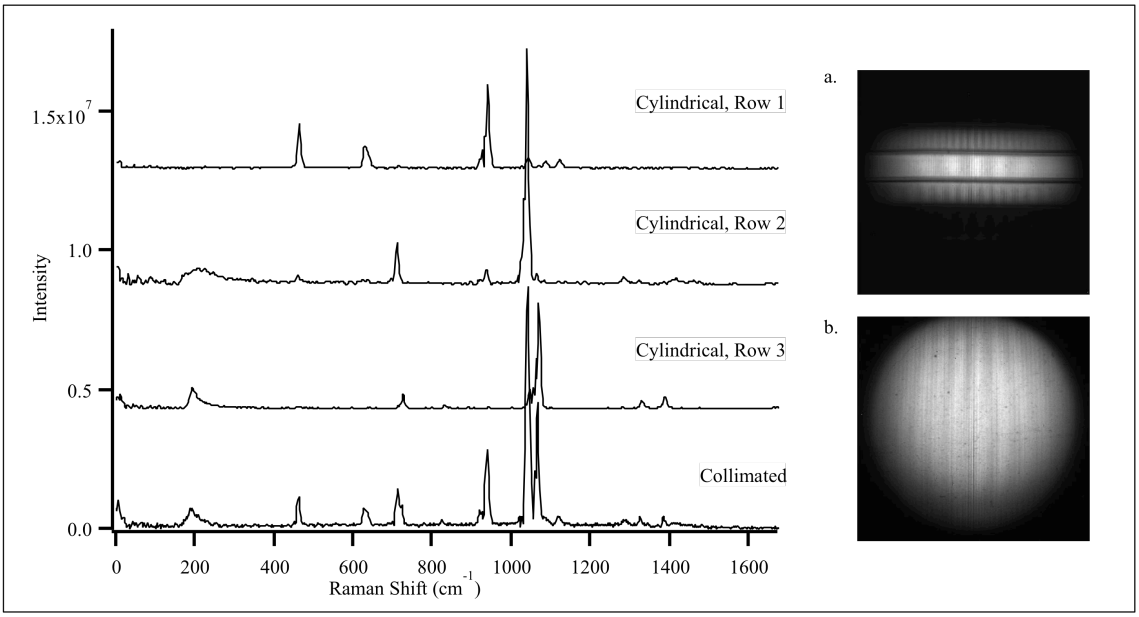

Figure 2.7: Raman spectra using a cylindrical lens for imaging and a collimated input beam for non-imaging were measured using ~1.15 W, 532 nm laser power illuminating the sample with a 3.5-4 cm beam diameter. The sample consisted of three vertically stacked 1 cm cuvettes containing $KClO_4$, NH_4NO_3, and a $NaNO_3/NaNO_2$ mixture. The Raman spectra labeled Cylindrical Rows 1-3 correspond to the three distinct rows in CCD image on the right measured with the cylindrical lens (a.). The Raman spectrum labeled Collimated corresponds to the CCD image on the right measured with the collimated beam (b.).

2.7 References

1. R.L. McCreery. Raman Spectroscopy for Chemical Analysis. New York, USA: Wiley, 2000.

2. S.P. Mulvaney, C.D. Keating. “Raman Spectroscopy.” Anal. Chem. 2000. 72(12): 145-158.

3. J. Cooney. ‘‘Satellite Observations Using Raman Component of Laser Backscatter.’’ In: R. Zirkind (ed.) Proceedings of the Symposium of Electromagnetic Sensing of the Earth from Satellites. New York, NY: Polytechnic Institute of Brooklyn Press, 1967, pp. P1–P10.

4. D.A. Leonard. ‘‘Observation of Raman Scattering from the Atmosphere using a Pulsed Nitrogen Ultraviolet Laser.’’ Nature. 1967. 216(5111): 142–143.

5. T. Hirschfeld. ‘‘Range Independence of Signal in Variable Focus Remote Raman Spectrometry.’’ Appl. Opt. 1974. 13(6): 1435–1437.

6. R.M. Measures. Laser Remote Sensing: Fundamentals and Applications. New York, USA: John Wiley & Sons, 1984.

7. S.M. Angel, T.J. Kulp, T.M. Vess. ‘‘Remote-Raman Spectroscopy at Intermediate Ranges Using Low-Power CW Lasers.’’ Appl. Spectrosc. 1992. 46(7): 1085–1091.

8. R.L. Aggarwal, L.W. Farrar, D.L. Polla. ‘‘Measurement of the Absolute Raman Scattering Cross Sections of Sulfur and the Standoff Raman Detection of a 6 mm thick Sulfur Specimen at 1500 m.’’ J. Raman Spectrosc. 2011. 42(3): 461–464.

9. P.G. Lucey, T.F. Cooney, S.K. Sharma. ‘‘A Remote Raman Analysis System for Planetary Landers.’’ Paper presented at: LPSC 1998. Houston, TX; March 16–20 1998.
10. K.A. Horton, N. Domergue-Schmidt, S.K. Sharma, P. Deb, P.G. Lucey. ‘‘Remote Raman System for Planetary Landers: Data Reduction and Analysis.’’ Paper presented at: LPSC 2000.Houston, TX; March 13–17 2000.
11. S.M. Angel, N.R. Gomer, S.K. Sharma, C. McKay. ‘‘Remote Raman Spectroscopy for Planetary Exploration: A Review.’’ Appl. Spectrosc. 2012. 66(2): 137–150.
12. M. Gaft, L. Nagli. ‘‘UV Gated Raman Spectroscopy for Standoff Detection of Explosives.’’ Opt. Mater. 2008. 30(11): 1739–1746.
13. J. Moros, J.A. Lorenzo, K. Novotny´, J.J. Laserna. ‘‘Fundamentals of Stand-off Raman Scattering Spectroscopy for Explosive Fingerprinting.’’ J. Raman Spectrosc. 2013. 44(1): 121–130.
14. A. Pettersson, S. Wallin, H. Ostmark, A. Ehlerding, I.Johansson, M. Nordberg, H. Ellis, A. Al-Khalili. ‘‘Explosives Standoff Detection using Raman Spectroscopy: from Bulk Towards Trace Detection.’’ Proc. SCIE. 2010.76641K: 1–12.
15. J.C. Carter, J. Scaffidi, S. Burnett, B. Vasser, S.K. Sharma, S.M. Angel. ‘‘Stand-off Raman Detection using Dispersive and Tunable Filter Based Systems.’’ Spectrochim. Acta, Part A. 2005. 61(10): 2288–2298.
16. J.C. Carter, S.M. Angel, M. Lawrence-Snyder, J. Scaffidi, R.E. Whipple, J.G. Reynolds. ‘‘Standoff Detection of High Explosive Materials at 50 Meters in

Ambient Light Conditions Using a Small Raman Instrument.'' Appl. Spectrosc. 2005. 59(6): 769–775.

17. M. Wu, M. Ray, K.H. Fung, M.W. Ruckman, D. Harder, A.J. Sedlacek. ''Stand-off Detection of Chemicals by UV Raman Spectroscopy.'' Appl. Spectrosc. 2000. 54(6): 800–806.
18. M.D. Ray, A.J. Sedlacek, M. Wu. ''Ultraviolet Mini-Raman Lidar for Stand-off, In Situ Identification of Chemical Surface Contaminants.'' Rev. Sci. Instrum. 2000. 71(9): 3485–3489.
19. M. Skulinova, C. Lefebvre, P. Sobron, E. Eshelman, M. Daly, J.-F. Gravel, J.F. Cormier, F. Chaˆteauneuf, G. Slater, W. Zheng, A. Koujelev, R. Leveille. ''Time-resolved Stand-off UV-Raman Spectroscopy for Planetary Exploration.'' Planet. Space Sci. 2014. 92: 88–100.
20. T.J. Kulp, S.E. Bisson, T.A. Reichardt. ''Standoff Ultraviolet Raman Scattering Detection of Trace Levels of Explosives.'' Sandia Natl. Lab. [Tech. Rep.] Sandia Report. 2011. 7955. doi:10.2172/1030305.
21. R.L. McCreery. ''Magnitude of Raman Scattering.'' In: T.D. Winefordner (ed.) Raman Spectroscopy for Chemical Analysis. New York, NY: John Wiley & Sons, Inc, 2000, pp.15–33.
22. S.A. Asher. ''UV Resonance Raman Spectroscopy for Analytical, Physical, and Biophysical Chemistry. Part 1.'' Anal. Chem. 1993. 65(2): 59A–66A.
23. M. Ghosh, L. Wang, S.A. Asher. ''Deep-Ultraviolet Resonance Raman Excitation Profiles of NH_4NO_3, PETN, TNT, HMX, and RDX.'' Appl. Spectrosc. 2012. 66(9): 1013–1021.

24. S.A. Asher, C.R. Johnson. ‘‘Raman Spectroscopy of a Coal Liquid Shows that Fluorescence Interference is Minimized with Ultraviolet Excitation.’’ Science. 1984. 225(4659): 311–313.

25. N.R. Gomer, C.M. Gordon, P. Lucey, S.K. Sharma, J.C. Carter, S.M. Angel. “Raman Spectroscopy Using a Spatial Heterodyne Spectrometer: Proof of Concept.” Appl. Spectrosc. 2011. 65(8): 849-857.

26. N. Lamsal, S.M. Angel. ‘‘Deep-Ultraviolet Raman Measurements Using a Spatial Heterodyne Raman Spectrometer (SHRS).’’ Appl. Spectrosc. 2015. 69(5): 525–534.

27. N. Lamsal, S.M. Angel, S.K. Sharma, T.E. Acosta. ‘‘Visible and UV Standoff Raman Measurements in Ambient Light Conditions Using a Gated Spatial Heterodyne Raman Spectrometer.’’ Abstract 1459, 46th LPSC 2015. Woodland TX; March 16-20, 2015.

28. N. Lamsal, S. K. Sharma, T. E. Acosta, S. M. Angel. “Ultraviolet Stand-off Raman Measurements Using a Gated Spatial Heterodyne Raman Spectrometer.” Appl. Spectrosc., in press 2016, DOI: 10.1177/0003702816631304.

29. P. D. Barnett, N. Lamsal, S. M. Angel. “Standoff LIBS using a Miniature Wide Field of View Spatial Heterodyne Spectrometer with Sub-Microsteradian Collection Optics.” Appl. Spectrosc. Submitted for publication February 2016.

30. J.M. Harlander. Spatial Heterodyne Spectroscopy: Interferometric Performance at any Wavelength Without Scanning. [Ph.D. Thesis]. Madison, WI: University of Wisconsin, 1991.

31. J.M. Harlander, F.L. Roesler, S. Chakrabarti. “Spatial Heterodyne Spectroscopy: A Novel Interferometric Technique for the FUV.” In: O.H.W. Siegmund, H.S. Hudson, editors. EUV, X-Ray, and Gamma-Ray Instrumentation for Astronomy. Proc. SPIE. 1990, 1344: 120-131.
32. J.M. Harlander, F.L. Roesler, J.G. Cardon, C.R. Englert, R.R. Conway. “Shimmer: A Spatial Heterodyne Spectrometer for Remote Sensing of Earth’s Middle Atomsphere.” Appl. Opt. 2002. 41(7): 1343-1352.
33. J. Harlander, R. Reynolds, F. Roesler. “Spatial Heterodyne Spectroscopy for the Exploration of Diffuse Interstellar Emission-Lines at Far-Ultraviolet Wavelengths.” Astrophys. J. 1992. 396(2): 730-740.
34. M. Prencipe, F. Pascale, C.M. Zicovich-Wilson, V.R. Sanders, R. Orlando, R. Dovesi. “The Vibrational Spectrum of Calcite ($CaCO_3$): an ab initio Quantum-Mechanical Calculation.” Phys. Chem. Minerals 2004. 31(8): 559-564.
35. J.F. Scott, S.P.S. Porto. “Longitudinal and Transverse Optical Lattice Vibrations in Quartz.” Phys. Rev. 1967. 161(3): 903-910.
36. A. Chopelas. “Single Crystal Raman Spectra of Forsterite, Fayalite, and Monticellite.” Am. Mineral. 1991. 76(7-8): 1101-1109.
37. C.P. Marshall, A.O. Marshall. “Challenges Analyzing Gypsum on Mars by Raman Spectroscopy.” Astrobiology 2015. 15(9): 761-769.
38. K.B. Mabrouk, T.H. Kauffman, H. Aroui, M.D. Fontana. “Raman Study of Cation Effect on Sulfate Vibration Modes in Solid State and in Aqueous Solutions.” J. Raman Spectrosc. 2013. 44(11): 1603-1608.

39. C. Shantakumari. “Raman Spectra of Crystalline Sulphates of Zinc, Magnesium and Sodium.” P. Indian. As-Math. Sci. 1953. 37(3): 393-400.

40. R.J. Bakker. “Raman Spectra of Fluid and Crystal Mixtures in the Systems H_2O, H_2O-NaCl and H_2O-$MgCl_2$ at Low Temperatures: Applications to Fluid-Inclusion Research.” Can. Mineral. 2004. 42(5): 1283-1314.

41. I. Durickovic, R. Claverie, P. Bourson, M. Marchetti, J.-M. Chassot, M.D. Fontana. “Water-ice Phase Transition Probed by Raman Spectroscopy.” J. Raman Spectrosc. 2011. 42(6): 1408-1412.

42. F. Hanke, U. Bottger, S.G. Pavlov, H.-W. Hubers. ‘‘Raman Spectra of Frozen Salt Solutions Relevant for Planetary Surfaces.’’ EPSC Abstracts. 2014. 9(EPSC2014): 403-1.

43. D. Oelkrug, M. Brun, P. Hubner, K. Rebner, B. Boldrini, R.W. Kessler. “Penetration of Light into Multiple Scattering Media: Model Calculations and Reflectance Experiments. Part II: the Radial Transfer. Appl. Spectrosc. 2012. 66(8): 934-943.

44. D. Oelkrug, E. Ostertag, R.W. Kessler. “Quantitative Raman Spectroscopy in Turbid Matter: Reflection or Transmission Mode?” Anal. Bioanal. Chem. 2013. 405(10): 3367-3379.

45. A. Wang, R.L. Korotev, B.L. Jolliff, Z. Ling. “Raman Imaging of Extraterrestrial Materials.” Planet. Space Sci. 2015. 112(July 2015): 23-34.

46. B.W. Smith, J.M. Harlander. “Imaging Spatial Heterodyne Spectroscopy: Theory and Practice.” Proc. SPIE. 1999. 3698: 925-930.

CHAPTER 3

TRANSMISSION RAMAN MEASUREMENTS USING A SPATIAL HETERODYNE RAMAN SPECTROMETER (SHRS)

[1] Strange, K.A., K.C. Paul, and S.M. Angel. In Press. *Applied Spectroscopy*,

Reprinted here with permission of publisher, 03/18/2016.

3.1 Abstract

A spatial heterodyne Raman spectrometer (SHRS) was used to measure transmission Raman spectra of highly scattering compounds. Transmission Raman spectral intensities of ibuprofen were only 2.4 times lower in intensity than backscatter Raman spectra. The throughput was about eight times higher than an f/1.8 dispersive spectrometer, and the width of the area viewed was found to be seven to nine times higher, using 50.8 mm and 250 mm focal length collection lenses. However, the signal-to-noise ratio was two times lower for the SHRS than the f/1.8 dispersive spectrometer, apparently due to high levels of stray light.

3.2 Introduction

Transmission Raman spectroscopy (TRS) provides nondestructive, noninvasive, and unique molecular identification of the bulk contents of a heterogeneous sample.[1-2] TRS has been shown to be a useful technique in various areas of research such as cancer diagnostics,[3] pharmaceutical qualification and quantification,[4] and process control applications.[5] Stone and Matousek demonstrated the ability to distinguish between benign and malignant markers of breast cancer tumors at clinically relevant depths using TRS.[3] Eliasson et al. conducted feasibility studies using TRS for quantitative analysis of pharmaceutical samples. The work demonstrated TRS, in combination with chemometrics, could be used to measure the active pharmaceutical ingredient concentration with ~1-2% relative error despite strong Raman signals from the capsule shell.[4] Macleod and Matousek reviewed TRS studies pertaining to using TRS for process control of pharmaceutical products.[5] The review describes how TRS can be used for fast,

quantitative, nondestructive process control measurements with high specificity of the bulk components for heterogeneous samples.

The TRS technique takes advantage of the diffuse scattering of Raman photons through a sample to increase the Raman signal from the bulk relative to the surface (i.e. reduced sub-sampling). Sub-sampling is the bias to surface layer constituents in backscatter Raman of highly scattering samples, which limits the ability to use backscatter Raman to obtain spectra that are representative of the bulk for highly scattering samples. In TRS, diffuse scattering of light increases interactions within the sample leading to spectra that are more representative of the bulk. However, this comes at the price of reducing the Raman signal compared to backscatter Raman.

In TRS, Raman scattered photons exit the sample in a very large area, in a spot about 6 times the sample thickness.[6-8] Typical dispersive spectrometers have small entrance slits and are not efficient at collecting light from a large area sample, which leads to low collection efficiency and reduced sensitivity in TRS in comparison to backscatter Raman. The backscatter/transmission (B/T) ratio is a measure of signal loss and is typically a large number for TRS, 10-100.[1-2,4,9] To increase the sensitivity in TRS measurements, signal enhancement techniques can be employed or the collection area can be increased. Signal enhancement has been achieved through the use of unidirectional coupling mirrors to recycle the Raman and laser photons lost on the non-collection sides of the sample.[10-11] Most TRS studies have used fiber optic bundles to increase the collection area, but the small diameter of the fibers still limits the total area that can be viewed, and typical B/T ratios using optical fibers for light collection are 10 to 18.[1-4,12] FT-Raman has also been demonstrated for TRS measurements as the throughput should

be larger than a typical dispersive spectrometer. However, Pelletier et al., using FT Raman for TRS, reported a 20 -100 times decrease in the transmission Raman intensity compared to the backscatter intensity, citing self-absorption at near-infrared (NIR) wavelengths and poor Raman collection efficiency.[9]

Recently, we demonstrated a new type of Fourier transform (FT) Raman spectrometer, the spatial heterodyne Raman spectrometer (SHRS), that has very high light throughput and a wide field-of-view.[13] The SHRS is well suited for measuring large sample areas and could be useful for TRS measurements. The purpose of this paper is to demonstrate TRS using the SHRS and to make comparisons to a more conventional, high throughput dispersive spectrometer.

3.3 Experimental

3.3.1 SHRS

Figure 3.1 (top) shows a schematic of the SHRS. The basic spectrometer design has been previously described.[13-16] For TRS, the SHRS uses a 25 mm cube beam splitter (CM1-BS013, ThorLabs) and two 25 mm, 150 grooves/mm gratings, blazed at 500 nm. A grating mount (DGM-1; Newport Corp.) was used to manually control the grating rotation and tilt, to precisely set the Littrow wavelength. A 105 mm focal length, f/2.8 lens (AF Micro-Nikkor; Nikon) was used to image the gratings at unity magnification onto a liquid nitrogen cooled charge-coupled device (CCD) detector with 1340 x 1300, 20 micron pixels (VersArray; Princeton Instruments). The CCD fringe image was recorded using Winspec (32-bit, version 2.5.22.0), and data processing was performed using Matlab (MathWorks, version R2013a) and IGOR Pro (WaveMetrics, version

6.03A2) software. In some cases, additional images were used for background corrections of the fringe images. This has been described previously.[14]

A 532 nm diode-pumped continuous wave (CW) laser (Millennia Pro 2s; Spectra-Physics) was used as the excitation source for all SHRS spectra presented, and was also used as a reference wavelength to set the Littrow angle of the gratings to 532 nm. Raman light was collected from the sample and directed into the SHRS using either an f/5 achromatic, 50.8 mm diameter, 250 mm focal length, MgF_2 coated lens (PAC088; Newport Corp.) or an f/2 achromatic, 25 mm diameter, 50.8mm focal length, MgF_2 coated lens (49766; Edmund Optics), L_1 in Figure 3.1. The collimated light was filtered using various combinations of three filters: a 600 nm short-pass filter (10SWF-600-B; Newport Corp.) to block out-of-band light, and 532 nm long-pass (LP03-532RE-25; Semrock) and 532 nm holographic filters (Supernotch; Kaiser Optical Systems Inc.) for laser line rejection. These filters limited the SHRS aperture to 22.8 mm.

3.3.2 Kaiser Holospec

The Kaiser Holospec f/1.8 Holographic Imaging spectrometer (Kaiser Optical Systems Inc.) is a very fast, commercially available visible Raman spectrometer and is used as a "worst case" comparison for the SHRS. The spectrometer was equipped with a low frequency 532 nm Stokes grating (HSG-532-LF; Kaiser Optical Systems Inc.) giving a spectral range of 50-2400 cm^{-1} with linear dispersion of 3.1 nm/mm. The slit width was either 25 or 100 mm giving a nominal spectral resolution of 3-11 cm^{-1}. For the Holospec field-of-view measurements, a ~150 mW, 532 nm diode laser (Solid state DP55L) was used, whereas for throughput and signal-to-noise studies the Spectra Physics laser was

used. As shown in Figure 3.1 (Lower), a 25 mm diameter, f/2 achromatic focusing lens was used to f/# match the Kaiser spectrometer. Collection lenses were identical to those used in the SHRS set-up. Note: for both the dispersive and SHRS instruments, when the larger diameter, longer focal length lens was used for light collection, about the same amount of light was lost to the spectrometer, by coupling mismatch to the 25-mm diameter focusing lens, in the case of the dispersive system, or coupling to the 22.8 mm aperture of the SHRS. Since the mismatch is the same for both spectrometers, it should not affect the results. With the dispersive instrument, a thermo-electrically cooled CCD detector with 1340 x 400, 20 micron pixels (Pixus 400; Princeton Instruments) was used. Spectra were collected and analyzed with Winspec, Matlab, and IGOR Pro software.

3.3.3 Samples

Potassium perchlorate, sodium nitrate, sodium nitrite, and ammonium nitrate were purchased from Sigma-Aldrich at 99%+ purity and used "as is." Acetaminophen (Good Sense®, Extra Strength 500 mg caplets) was purchased as an over-the-counter pharmaceutical, and the thin coating was scraped off before analysis in the hopes of reducing fluorescence from the coating. Removing the coating was later found to have little effect on fluorescence in the Raman spectrum. Ibuprofen, 99%, was purchased from Acros Organics. Ibuprofen and perchlorate pellets were made by grinding the samples using a mortar and pestle, then pressed with a hydraulic pellet press (Carver Laboratory Equipment, model 3912) with a 13 mm stainless steel pellet dye.

3.4 Results and discussion

3.4.1 SHRS

The SHRS is similar to a Michelson interferometer with stationary gratings used in the place of moving mirrors, see Figure 3.1. The Raman signal from the sample is collimated and directed into the interferometer, where it is split into two beams and directed to the gratings in each arm of the interferometer. The gratings are tilted at a specific angle, the Littrow angle θ_L, so that at one wavelength (i.e., the Littrow wavelength) the light is exactly retro-reflected. All other wavelengths are heterodyned to the Littrow wavelength and form a wavelength dependent interference pattern of vertical fringes which is imaged onto the CCD.[17-18] The columns of the fringe image are typically integrated to make the fringe cross section, and the Fourier transform of the fringe cross section produces the Raman spectrum. In the interferogram, the fringe spacing is defined by:

$$f = 4(\sigma - \sigma_L)\tan\theta_L \qquad \text{Equation 3.1}$$

where f is in fringes per centimeter, σ is the wavenumber of the Raman band, and σ_L is the Littrow wavenumber. The intensity of the fringe pattern is a function of position x on the detector, given by:

$$I(x) = \int_0^\infty B(\sigma)\{1 + \cos[8\pi(\sigma - \sigma_L)x\tan\theta_L]\}d\sigma \qquad \text{Equation 3.2}$$

where $B(\sigma)$ is the input spectral intensity at wavenumber σ, and the Fourier transform of $I(x)$ yields the Raman spectrum.[17-20]

Unlike a dispersive spectrometer, the resolution of the SHRS is not a strong function of the entrance aperture. So large apertures can be used to provide very high throughput, without sacrificing spectral resolution. The resolving power (R) of the SHRS is equal to the total number of grating grooves illuminated, about 6840 for the system used here with a 22.8 mm clear aperture (limited by the filters). The resolving power gives a nominal 2.6 cm^{-1} spectral resolution,[17] about the same as the f/1.8 spectrometer with 25 mm slit. The spectral resolution of the SHRS was measured with a Hg lamp to be ~8 cm^{-1}. The resolution of the SHRS can be affected by non-optimal camera focusing, poor collimation of input beam, optical defects in gratings, and poor quality imaging optics.

The Etendue of a spectrometer is a function of the area viewed and the collection solid angle. The collection solid angle of the SHRS, Ω_S, is defined in Equation 3.[17]

$$\Omega_S = 2\pi/R \qquad \text{Equation 3.3}$$

For the system used here, the collection solid angle is about 9.2 x 10^{-4} sr, giving an acceptance angle (or field of view, FOV) of ~3 x 10^{-2} radians (i.e. 1.7°). For small angles, the width of the area viewed by the SHRS is the product of the instrument acceptance angle and the distance to the sample. Thus, for the 250 mm and 50.8 mm focal length lenses, the width of the area viewed on the sample would be 7.6 mm and 1.5 mm, respectively. The Etendue of the SHRS with a 22.8 mm aperture is then 0.38 $mm^2 \cdot sr$. For the f/1.8 dispersive spectrometer with a 25 mm slit, the Etendue is 0.048 $mm^2 \cdot sr$, about 8 times lower than the SHRS.

3.4.2 Representative TRS spectra measured with the SHRS

Figure 3.2 shows transmission Raman spectra measured using the SHRS of some highly scattering samples, an over-the-counter acetaminophen tablet, ammonium nitrate, sodium nitrate/sodium nitrite mixture, and potassium perchlorate, as well as the corresponding fringe image cross sections for each sample (upper left inset). The TRS spectra of the unground salts were measured with the samples in 1 cm quartz cuvettes. The over-the-counter acetaminophen tablet was measured as-is, after scraping off the thin coating. The measured spectral resolution for the sample Raman bands ranged from 8.4 to 10 cm^{-1}; a little larger than the measured resolution of the instrument.

The fringe visibility (FV, see Equation 4) of the interferograms shown in the inset are ~0.10, 0.17, 0.18, and 0.36 for the acetaminophen, ammonium nitrate, sodium nitrate/sodium nitrite, and potassium perchlorate, respectively. Fringe visibility is a measure of the modulation efficiency of the interferometer and low values can indicate poor interferometer alignment or high levels of background light outside the range of the interferometer. Low FV can also be the result of nonuniform illumination on the CCD, and this can be corrected by flat field corrections. However, no flat field or any other corrections were done to the images for the data shown. The indicated values are less than typical FV values reported for visible FT Raman systems, suggesting high background light and non-optimal alignment of the SHRS interferometer.[21]

$$FV = (I_{max} - I_{min})/(I_{max}+I_{min}) \qquad \text{Equation 3.4}$$

High levels of background light in the SHRS seem to be the main source of the relatively low FV values measured. Background sources can include unblocked ambient

room light, sample fluorescence, and unblocked laser light. Ambient light was eliminated by making the measurements in a dark room. Fluorescence was not observed in the Raman spectra of the high purity salt samples. However, the acetaminophen spectrum shows some fluorescence, which is not uncommon for organic samples measured using a 532 nm laser. The high background in the fringe cross sections is likely from unblocked laser light scattering inside the instrument and reaching the detector. Poor fringe visibility increases noise in the SHRS spectra and is a current limitation of the SHRS used for these studies.

3.4.3 Backscatter/transmission comparison

The sample arrangements for transmission (a) and backscattered (b) Raman measurements are shown in Figure 3.1. In TRS, the laser is brought in from the backside of the sample, and laser and Raman photons are scattered diffusely through the sample and collected on the opposite side. The TRS sampling geometry averages the Raman signal from all depths in the sample and reduces surface layer bias. For highly diffuse scattering samples, TRS can lead to reduced scattered laser light in the Raman spectrum.[1,22]

Figure 3.3 shows backscatter and transmission Raman spectra of a 13 mm diameter, 4.36 mm thick ibuprofen pellet measured with the SHRS. The measured vibrational frequencies in the Raman spectra shown match the theoretical and experimental data of Jubert, et al.[23] The transmission Raman intensity was found to be only 2.4 times lower than the backscatter Raman intensity. This B/T ratio is much smaller

than typical values reported for TRS which range from 10 to 100.[1-2,4,9] The smaller ratio reported here results from the larger field-of-view of the SHRS.

3.4.4 Width of the area viewed

Figures 3.4 and 3.5 show the experimentally measured width of the area viewed by the SHRS and the f/1.8 dispersive system using 250 mm and 50.8 mm focal length collection lenses, respectively. The width of the area viewed was determined by moving a razor edge across the sample and measuring the Raman intensity of the sample at each position. The diameter of the area viewed was taken as the distance between the 5% and 95% values in the fitted curve. A 7 mm thick x 13 mm diameter $KClO_4$ pellet was used for these measurements, except for the SHRS 250 mm focal length lens experiment, where the powder sample was held in a 10 mm cuvette. The diameter of the illuminated spot on the samples, facing the spectrometer, was larger than the area viewed by either spectrometer. A 100 μm slit was used in the dispersive spectrometer for these studies to achieve the largest possible area viewed, for a "worst case" comparison to the SHRS. With a 100 μm slit, the spectral resolution of the dispersive system is ~10 cm^{-1}, and the calculated width of the area viewed, with 250 mm and 50.8 mm focal length lenses, should be 500 μm and 100 μm, respectively.

The measured width of the area viewed by the SHRS was 7.2 mm and 1.3 mm with the 250 mm and 50.8 mm focal length lenses, respectively, very close to the predicted values of 7.6 and 1.5 mm. The width of the area viewed by the dispersive system was 840 μm and 180 μm with the 250 mm and 50.8 mm focal length lenses, respectively, about twice the predicted values. The difference in the width of the area

viewed for the dispersive system is attributed to the thickness and misalignment of the razor edge at the sample surface. These errors are more pronounced in the dispersive spectrometer, because the width of the area viewed is very small. Therefore, the measured width of the area viewed by the SHRS is about nine and seven times larger than the width of the area viewed by the f/1.8 dispersive spectrometer, using 250 mm and 50.8 mm focal length lenses, respectively.

3.4.5 Throughput

As shown above, the Etendue of the SHRS is about eight times larger than the dispersive spectrometer, assuming the entire 8 mm high slit of the dispersive spectrometer is illuminated. Figure 3.6 shows Raman spectra of ibuprofen, five measured with the SHRS and five measured with the f/1.8 dispersive system, using identical collection optics. The reproducibility and SNR are so high that each of the five overlap exactly on this scale. The dispersive spectrometer slit width was set to 0.025 mm to match the resolution of the SHRS. For these measurements, all experimental parameters were the same except for the CCD gain, which was 1 and 4 photoelectrons/count for the dispersive system and the SHRS, respectively. In the inset, the spectra are shown over the full wavelength range, and the SHRS spectral intensity is shown multiplied by 4 to compensate for lower CCD gain. The average baseline subtracted peak intensity (i.e. counts) for the 830 cm^{-1} band of ibuprofen was two times higher for the SHRS than the dispersive system (the area of the bands gave similar result). Correcting for the lower gain of the SHRS detector, the measured light throughput of the SHRS was about eight times larger than the dispersive system, which matches the calculated values.

3.4.6 Signal-to-noise

Using the 830 cm^{-1} Raman band of ibuprofen in the spectra shown in Figure 3.6, the signal-to-noise ratio (SNR) was compared for both systems. It is difficult to compare absolute values of SNR between the two systems, because the noise is distributed differently. To compare relative noise levels, the ratio of replicate spectra for each system were compared (solid and dashed lines, labeled Ratios in Figure 3.6). The magnitude of the noise in the ratio spectra was 4-5 times higher for the spectra measured using the SHRS than the dispersive system. But the signal was ~2 times higher using the SHRS system, thus the SNR was about 2-2.5 times higher using the dispersive system. The throughput of the SHRS was 8-9 times higher than the dispersive system, and this might be expected to lead to a higher SNR, of ~3. The actual SNR of the SHRS is lower for a couple of reasons. For one thing, the FV of the system was lower than expected because of high background light. As shown in the Figure 3.2 inset, only a small part of the total collected light contributed to the interferogram, ~ 4% in the case of the potassium perchlorate spectrum. The remaining ~ 96% still contributes to noise in the spectrum. If the background could be reduced to zero, the SNR could potentially be improved about five-fold. Another reason for lower than expected SNR in the SHRS has to do with the large number of Raman bands in the spectra that were used for comparison. The area of the 830 cm^{-1} band is about 10% of the integrated area of all the bands in the spectral region shown. This is almost a "worst case" in terms of SNR. The noise is distributed equally in an interferometer, so the noise of the 830 cm^{-1} band is expected to be ~3 times higher than a dispersive system for equal signal levels. This factor of three almost cancels out the higher SHRS throughput.

3.5 Conclusions

A spatial heterodyne Raman spectrometer (SHRS) has been used to measure transmission Raman spectra of several highly scattering samples. The results demonstrate a larger throughput is achieved with the SHRS in comparison to a fast, f/1.8 dispersive spectrometer. The measured sample area viewed is also 7-9 times larger using the SHRS, and larger area viewed leads to a backscatter/transmission ratio of about 2.4, which is very low for a TRS measurement. The SNR of the SHRS is slightly less than the f/1.8 dispersive spectrometer for identical measurement conditions. The SNR of the SHRS used for these comparisons was limited by low fringe visibility, in large part caused by high background signals. More careful attention to the design of the spectrometer to reduce stray light should substantially improve the SNR and sensitivity of the spectrometer.

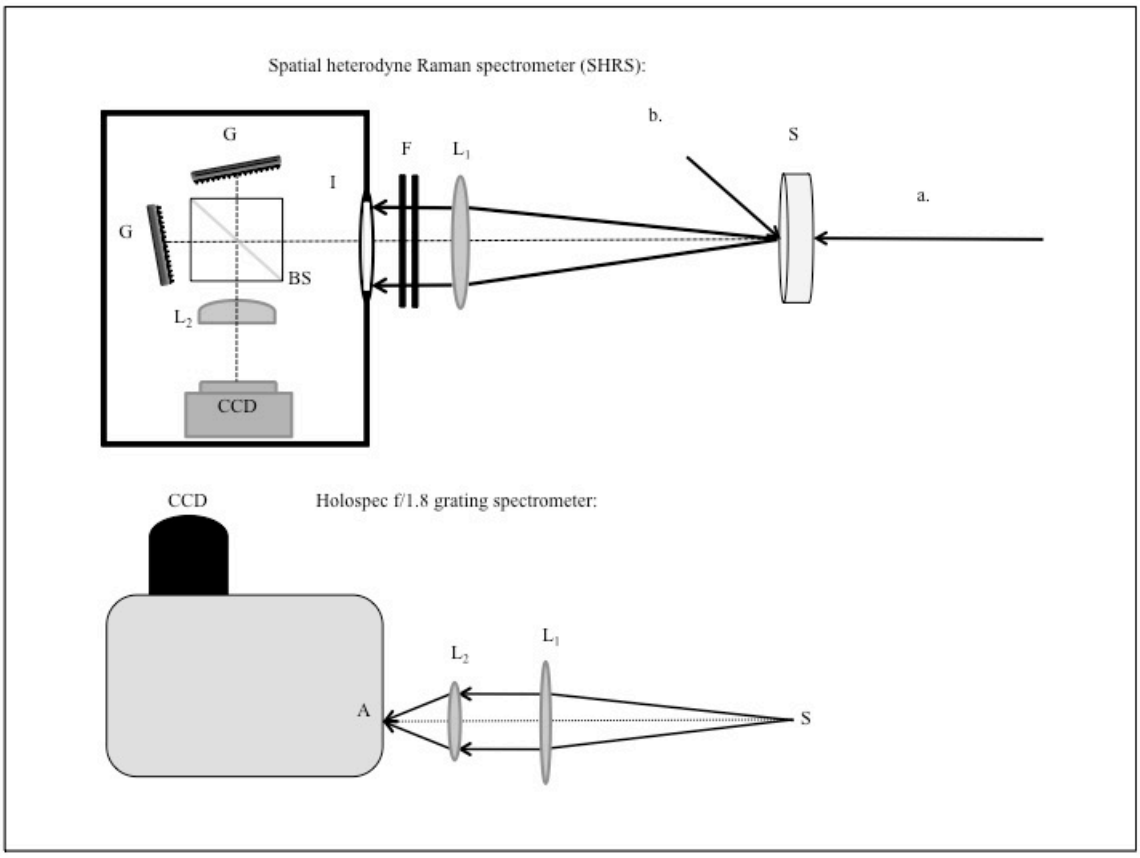

Figure 3.1

SHRS schematic- The Raman light collected by L_1 is directed through the filters (F) and into the input aperture (I), and the light is split 50/50 by the beam splitter (BS). The gratings (G) disperse the light and send it back towards the beam splitter, where the beams recombine. The imaging lens (L_2) focuses the image plane onto the CCD detector.

Kaiser Holospec f/1.8 dispersive spectrometer- The Raman scatter is collected with the collection lens (L_1), which collimates the light. The coupling lens (L_2) focuses the collimated light into the entrance slit (A) of the spectrometer.

a. Transmission Raman geometry
b. Backscatter Raman geometry

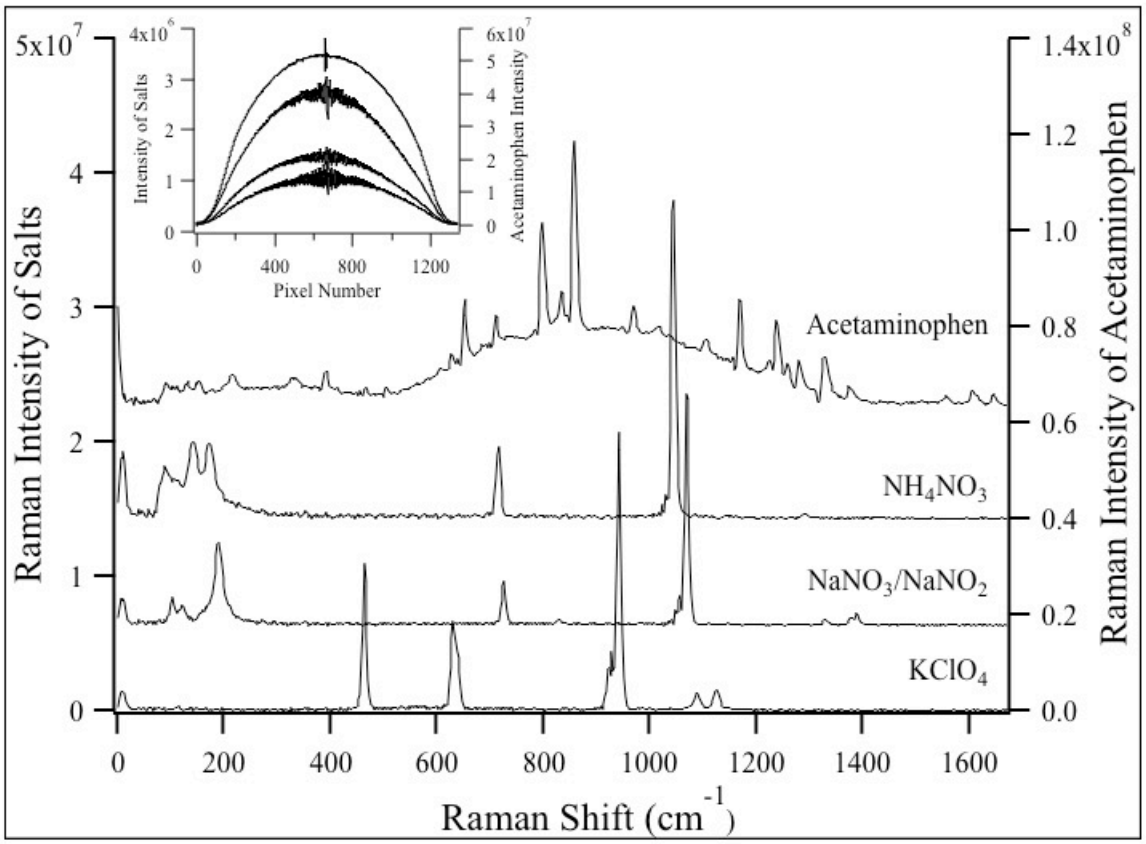

Figure 3.2

Transmission Raman spectra of acetaminophen, ammonium nitrate, a sodium nitrate/sodium nitrite mixture, and potassium perchlorate (from top to lower). The salts were measured in 1 cm cuvettes using 10 seconds acquisitions with a 1 W, 532 nm laser, and the acetaminophen tablet was measured using 90 seconds acquisition with ~200 mW laser power. Spectra offset for clarity. The fringe image cross sections are inset in the upper left hand corner and the order is identical to the spectra. The acetaminophen fringe cross section was background subtracted before generating the Raman spectrum.

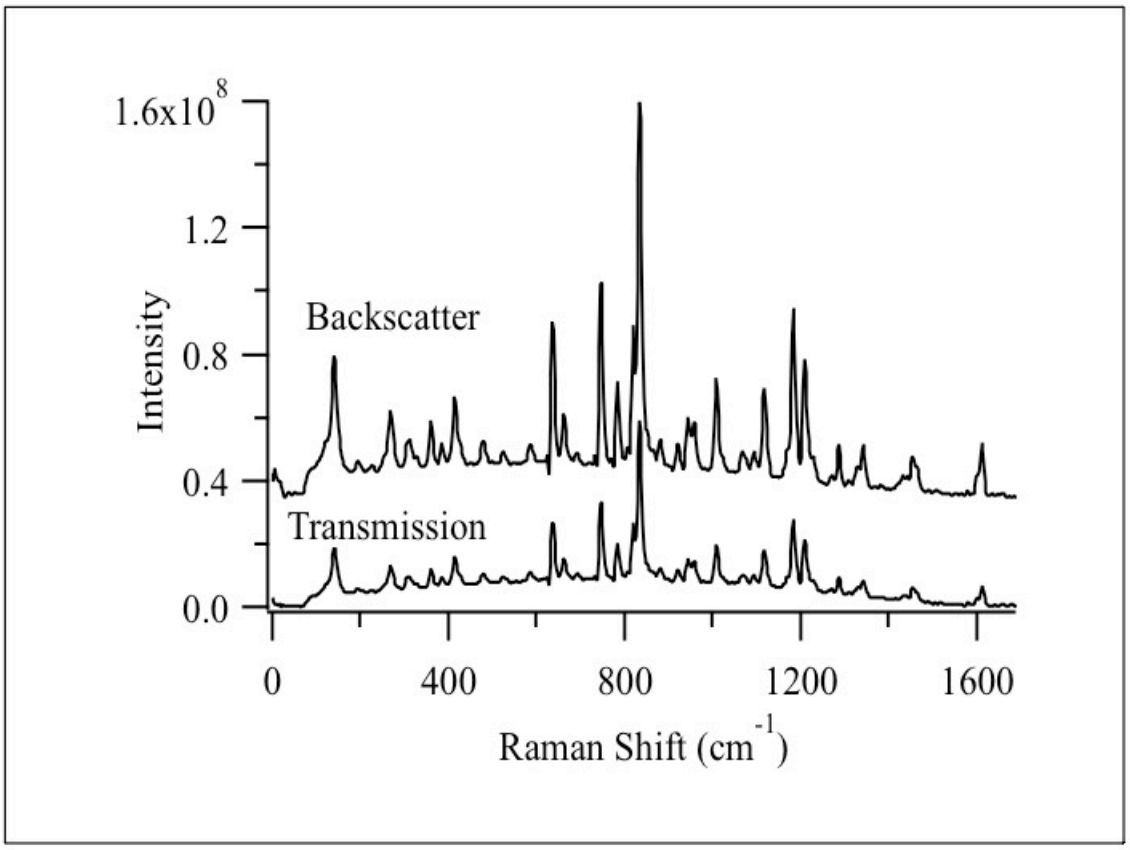

Figure 3.3

Transmission (lower) and backscatter (top) Raman spectra of ibuprofen pellet (4.4 mm thick, 13 mm diameter) measured with the SHRS using 60 second acquisition time and 460 mW. The backscatter spectrum was offset for clarity.

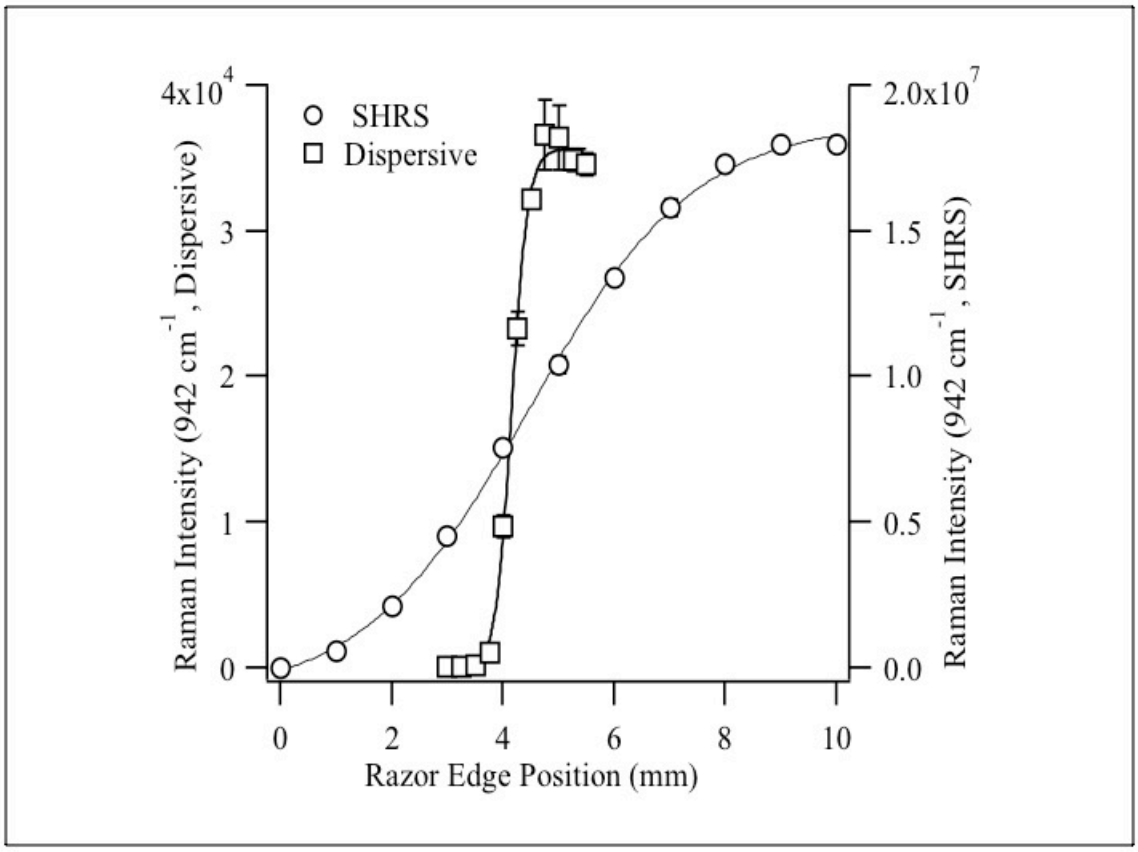

Figure 3.4

Width of the area viewed, showing Raman intensity versus position of razor edge, measured using a 250 mm focal length lens as the collection optic for the SHRS (circles) and f/1.8 dispersive spectrometer (squares). A $KClO_4$ sample was used for these measurements. The sample thickness was 10 x 10 mm for the SHRS experiment and 7 x 13 mm for the dispersive experiment.

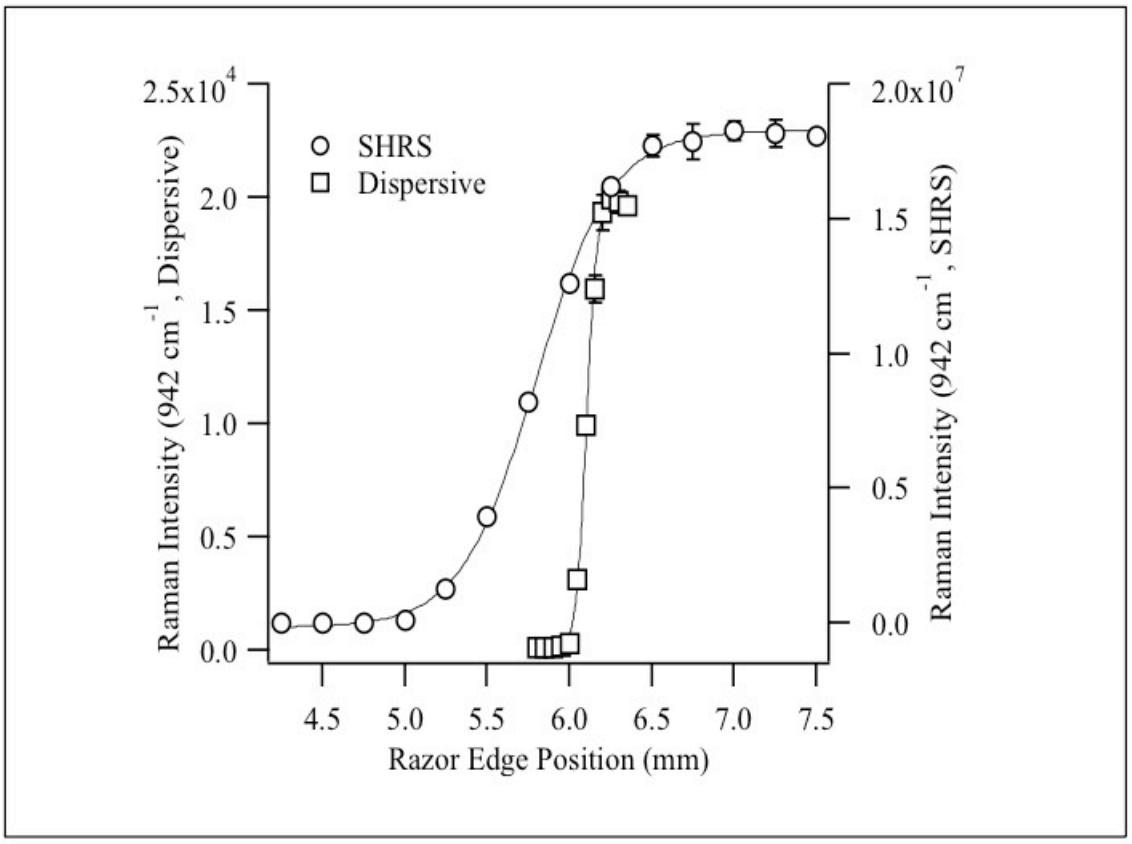

Figure 3.5

Width of the area viewed, showing Raman intensity versus position of razor edge, measured using a 50.8 mm focal length lens as the collection optic for the SHRS (circles) and f/1.8 dispersive spectrometer (squares). A 7 x 13 mm $KClO_4$ pellet was used for these measurements.

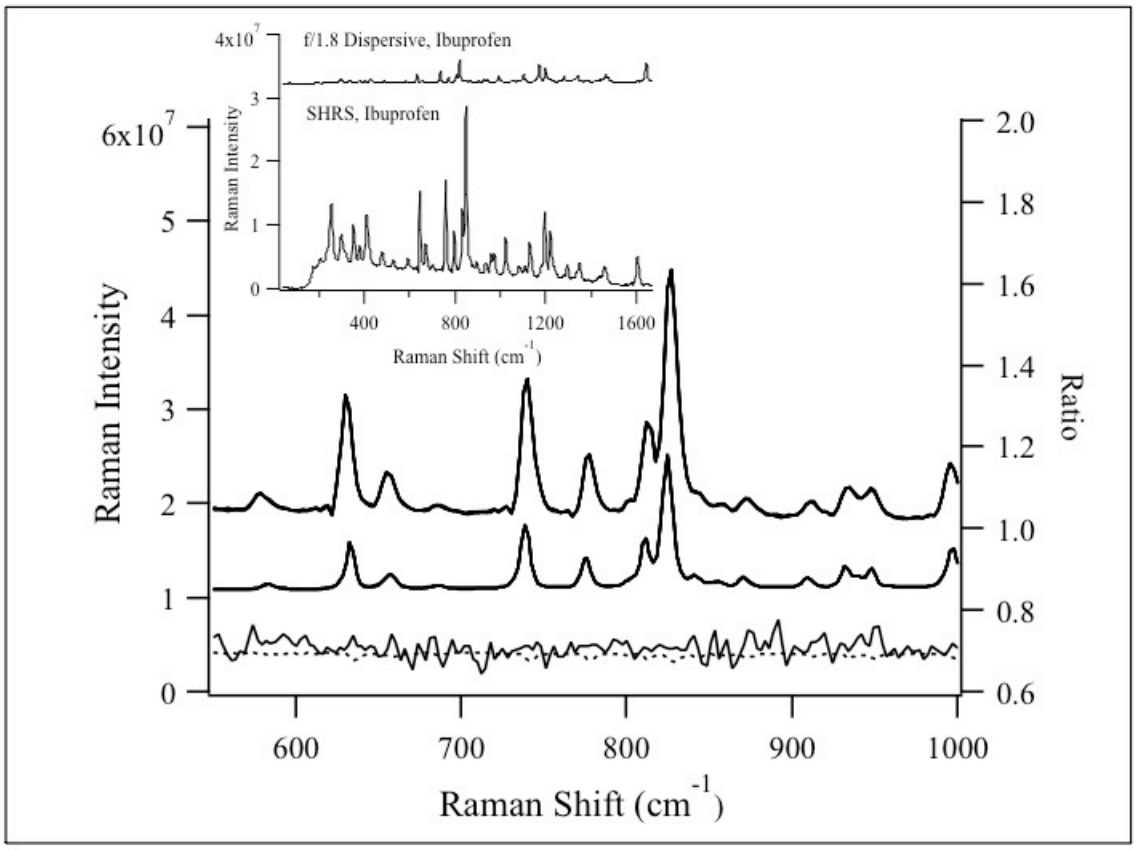

Figure 3.6

Transmission Raman spectra of ibuprofen measured with the f/1.8 dispersive spectrometer (lower) and the SHRS (top). Five replicate measurements with each spectrometer are shown. The ratio of replicate measurements is shown for the SHRS (solid line) and the dispersive spectrometer (dashed line). Inset: shows the SHRS spectrum corrected for CCD gain (i.e. intensity x 4), as well as a dispersive spectrum, over the full spectral range. The spectra were measured with 200 mW laser power using100 second acquisition time and a 250 mm focal length lens.

3.6 References

1. P. Matousek, A.W. Parker. “Bulk Raman Analysis of Pharmaceutical Tablets.” Appl. Spectrosc. 2006. 60(12): 1353-1357.
2. J. Johansson, A. Sparen, O. Svensson, S. Folestad, M. Claybourn. “ Quantitative Transmission Raman Spectroscopy of Pharmaceutical Tablets and Capsules.” Appl. Spectrosc. 2007. 61(11): 1211-1218.
3. N. Stone, P. Matousek. “Advanced Transmission Raman Spectroscopy: A Promising Tool for Breast Disease Diagnosis.” Cancer Res. 2008. 68(11): 4424-4430.
4. C. Eliasson, N.A. Macleod, L.C. Jayes, F.C. Clarke, S.V. Hammond, M.R. Smith, P. Matousek. “Non-invasive Quantitative Assessment of the Content of Pharmaceutical Capsules Using Transmission Raman Spectroscopy.” J. Pharm. Biomed. Anal. 2008. 47(2): 221-229.
5. N.A. Macleod, P. Matousek. “Emerging Non-invasive Raman Methods in Process Control and Forensic Applications.” Pharmaceut. Res. 2008. 25(1): 2205-2215.
6. N. Everall, P. Matousek, N. MacLeod, K.L Ronayne, I.P. Clark. “Temporal and Spatial Resolution in Transmission Raman Spectroscopy.” Appl. Spectrosc. 2010. 64(1): 52-60.
7. N. Everall, I. Priestnall, P. Dallin, J. Andrews, I. Lewis, K. Davis, H. Owen, M.W. George. “Measurement of Spatial Resolution and Sensitivity in Transmission and Backscattering Raman Spectroscopy of Opaque Samples: Impact on Pharmaceutical Quality Control and Raman Tomography.” Appl. Spectrosc. 2010. 64(5): 476-484.

8. D. Oelkrug, E. Ostertag, R.W. Kessler. “Quantitative Raman Spectroscopy in Turbid Matter: Reflection or Transmission Mode?” Anal. Bioanal. Chem. 2013. 405(10): 3367-3379.
9. M.J. Pelletier, P. Larkin, M. Santangelo. “Transmission Fourier Transform Raman Spectroscopy of Pharmaceutical Tablet Core.” Appl. Spectrosc. 2012. 66(4): 451-457.
10. M.J. Pelletier. “Sensitivity-Enhanced Transmission Raman Spectroscopy.” Appl. Spectrosc. 2013. 67(8): 829-840.
11. P. Matousek. “Raman Signal Enhancement in Deep Spectroscopy of Turbid Media.” Appl. Spectrosc. 2007. 61(8): 845-854.
12. K. Shin, H. Chung. “ Wide Area Coverage Raman Spectroscopy for Reliable Quantitative Analysis and its Applications.” Analyst 2013. 138(12): 3335-3346.
13. N.R. Gomer, C.M. Gordon, P. Lucey, S.K. Sharma, J.C. Carter, S.M. Angel. “Raman Spectroscopy Using a Spatial Heterodyne Spectrometer: Proof of Concept.” Appl. Spectrosc. 2011. 65(8): 849-857.
14. N. Lamsal, S. M. Angel. “Deep-Ultraviolet Raman Measurements Using a Spatial Heterodyne Raman Spectrometer (SHRS)”. Appl. Spectrosc. 2015. 69(5): 525–534.
15. N. Lamsal, S. M. Angel, S. K. Sharma, T. E. Acosta. “Visible and UV Standoff Raman Measurements in Ambient Light Conditions Using a Gated Spatial Heterodyne Raman Spectrometer”. Abstract 1459, 46th LPSC 2015. Woodland TX; March 16-20, 2015.

16. N. Lamsal, S. K. Sharma, T. E. Acosta, S. M. Angel. “Ultraviolet Stand-off Raman Measurements Using a Gated Spatial Heterodyne Raman Spectrometer”. Appl. Spectrosc., in press 2016, DOI: 10.1177/0003702816631304.
17. J.M. Harlander. Spatial Heterodyne Spectroscopy: Interferometric Performance at any Wavelength Without Scanning. [Ph.D. Thesis]. Madison, WI: University of Wisconsin, 1991.
18. J.M. Harlander, F.L. Roesler, S. Chakrabarti. “Spatial Heterodyne Spectroscopy: A Novel Interferometric Technique for the FUV.” In: O.H.W. Siegmund, H.S. Hudson, editors. EUV, X-Ray, and Gamma-Ray Instrumentation for Astronomy. Proc. SPIE. 1990, 1344: 120-131.
19. J.M. Harlander, F.L. Roesler, J.G. Cardon, C.R. Englert, R.R. Conway. “Shimmer: A Spatial Heterodyne Spectrometer for Remote Sensing of Earth’s Middle Atomsphere.” Appl. Opt. 2002. 41(7): 1343-1352.
20. J. Harlander, R. Reynolds, F. Roesler. “Spatial Heterodyne Spectroscopy for the Exploration of Diffuse Interstellar Emission-Lines at Far-Ultraviolet Wavelengths.” Astrophys. J. 1992. 396(2): 730-740.
21. R. Savoie, P. Beauchesne, D. Levesque. “Fourier Transform Raman Spectroscopy in the Visible Region.” Microchim. Acta. 1988. 95(1): 223-225.
22. N. Everall, T. Hahn, P. Matousek, A. W. Parker, M. Towrie. “Picosecond Time-Resolved Raman Spectroscopy of Solids: Capabilities and Limitations for Fluorescence Rejection and the Influence of Diffuse Reflectance.” Appl. Spectrosc. 2001. 55(12): 1701–1708.

23. A. Jubert, M.L. Legarto, N.E. Massa, L.L. Tevez, N.B. Okulik. “Vibrational and Theoretical Studies of Non-steroidal Anti-inflammatory Drugs Ibuprofen [2-(4-isobutylphenyl) propionic acid]; Napoxen [6-methoxy-α-methyl-2-naphthalene acetic acid] and Tolmetin Acids [1-methyl-5-(4methylbenzoyl)-1H-pyrrole-2-acetic acid]. J. Mol. Struct. 2006. 783(1-3): 34-5.

CHAPTER 4

ALL-REFRACTIVE SPATIAL HETERODYNE RAMAN SPECTROMETER (SHRS): PRELIMINARY RESULTS

4.1 Introduction

The spatial heterodyne Raman spectrometer (SHRS) has many benefits as outlined in Chapter 1. The grating SHRS is one variation of a spatial heterodyne spectrometer (SHS) investigated by our lab. Another variation, the all-refractive spatial heterodyne spectrometer, has a prism and mirror pair in each arm of the interferometer instead of gratings, see Figure 4.1.[1] Our group also investigated the all-refractive SHS as a potential spectrometer for Raman spectroscopy.

Prisms can offer several other advantages over gratings such as no order overlap, increased throughput, and greater dispersion in the UV than the visible spectral region.[2] Unlike gratings that lose light to the unused orders produced by diffraction, prism dispersion is based on refraction and does not have orders, so the throughput can be higher. Grating efficiency for most commercially available gratings is between ~40-50% and ~70-80% in the UV and visible spectral regions, respectively. Whereas, an anti-reflection coated prism typically transmits 90% or more of the input light, with some light loss at the air/prism interface. One possible benefit of prisms having greater dispersion in the UV is the lower costs of more commercially available large apex angle prisms, but the geometric alignment may reduce spectral bandpass, as will be discussed in more detail below.

Order overlap occurs when the diffracted orders of polychromatic light spatially overlap and degrade the fringe image on the CCD, Figure 4.2. Several approaches to reducing order overlap in the grating system include spatial filtering between the imaging lens and CCD, spatially separating the orders by moving the gratings away from the beam

splitter, or by changing the dispersive element in the SHRS to one that does not disperse light into orders. Spatial filtering works well at reducing order overlap, but the extra orders traveling through the beam splitter can add scattered light and increase background noise. A moderate resolution (150 grooves/mm) grating with a Littrow angle set to 532 nm diffracts first order at 2.3° and second order at 4.6°, which would require a distance of 305 mm to spatially separate the orders, see Figure 4.2. The same grating used at a Littrow angle set to 244 nm would diffract first and second order at 1.1° and 2.1°, respectively, requiring a distance of 686 mm to separate. Therefore, the overall size of the SHRS has to be greatly increased to spatially separate the orders before the beams recombine at the beam splitter. The SHRS can be miniaturized using high dispersion gratings, but as the size of the instrument decreases, so does the throughput. If high throughput is the most important aspect of the spectrometer, then the all-refractive SHS may be a good option.

4.2 All-Refractive SHRS

An all-refractive SHRS is governed by the same principles described in Chapter 1 for the grating-based SHRS. The input light is split 50/50 at the beam splitter and directed to each arm of the interferometer. The light is refracted through the prisms and is reflected by the mirror back through prism towards the beam splitter where the beams recombine. A fringe pattern is formed and imaged onto the CCD. The only difference between the two systems is how the light is dispersed.

Prism dispersion is a change in refractive index as a function of the wavelength and depends on the angle of deviation, δ, of a light ray from the light ray's original

optical path before entering a prism, Figure 4.3 (a.).[3] Using Snell's law and geometry, the deviation angle can be calculated by Equation 4.1,[2-4]

$$\delta = \gamma_i - \alpha + \sin^{-1}[(\sqrt{n^2 - \sin^2(\gamma_i)}) \cdot \sin(\alpha) - \cos(\alpha) \cdot \sin(\gamma_i)] \quad \text{Equation 4.1}$$

where γ_i is the angle of incidence, n is the refractive index, and α is the apex angle. The refractive index is dependent on the prism material and the wavelength of light, thus each wavelength will exit the prism at a different angle.

The angle of incidence can be set so that the exit light ray has the same angle as the incident light ray with respect to the normal of the prism face, which is called the angle of minimum deviation, Figure 4.3 (b.). Because the refractive index varies with wavelength, only one wavelength can be set to minimum deviation and travel through the prism symmetrically. In the SHRS, one wavelength is designated as the Littrow wavelength and completely refro-reflects through the system. When using prisms as the dispersing element in the SHRS, the Littrow angle of incidence, γ_L, is set to the angle of minimum deviation using Equation 4.2.[1]

$$n_L \sin(\alpha/2) = \sin(\gamma_L) \quad \text{Equation 4.2}$$

The resolving power for an all-refractive SHRS is dependent on the width of the illuminated area, W, of the prism,[1]

$$R_0 = 8W[\tan\gamma_L n_i^{-1}(\Delta n_i/\Delta\lambda) - \tan\gamma_F n_F^{-1}(\Delta n_F/\Delta\lambda)] \quad \text{Equation 4.3}$$

where $\Delta n/\Delta\lambda$ is the dispersion of the prism, and the subscripts i and f indicate the dispersing and field-widening prisms, respectively. The dispersing prism is made from a high dispersion material to increase the resolving power, and the field-widening prism is

made from a low dispersion material to optically adjust the image to appear geometrically parallel to the CCD plane without greatly reducing the dispersion. If there are no field-widening prisms used, as with the proto-types built in our lab, the equation for resolving power simplifies to Equation 4.4.[1]

$$R_0 = 4W[\tan\gamma_L n_i^{-1}(\Delta n_i/\Delta\lambda)] \qquad \text{Equation 4.4}$$

The dependence of the resolving power on the apex angle of the prism is not directly apparent from Equation 4.4. However, γ_L is determined by the apex angle of the prism, and the resolving power of the all-refractive SHRS will change with apex angle. The resolving power and angle of incidence are directly proportional to the prism apex angle. As the angle of incidence increases, so does the angle at which the reflecting mirror must be tilted to retro-reflect the dispersed light back through the prism. Large mirror tilts can lead to light loss and decreased bandpass as less refracted wavelengths will not travel back through the prism, Figure 4.4. Therefore, geometric considerations must be taken into account when choosing the prism apex angle.

4.3 Preliminary Results

4.3.1 All-refractive SHRS Prototype 1

As shown in Figure 4.1, two proto-types of all-refractive SHRS systems were designed and constructed for Raman spectroscopic measurements. For one proto-type (Figure 4.1, (a.)), a right angle prism with a mirror-coated back was used to reduce the degree of freedom and aid in easier alignment. The second proto-type (Figure 4.1, (b.)) used right angle prisms paired with mirrors so the zero path difference could be set using the mirrors and to reduce the thickness of the prism.

Proto-type one was the first to be constructed using right angle prisms with a mirror-coated back (Edmund Optics, 30-60-90 prism, #43673), coated-prism The Littrow wavelength was set to 532 nm and the entrance aperture was ~2.54 cm, giving a theoretical resolving power of 3700. The reflections of the laser off the face of the prism and mirror/prism interface were used to set the Littrow angle and align the prism in the xy plane of the optical axis using targets set at the height of the interferometer. Zero path difference (ZPD) could not be set as in a grating-based SHRS, where the zero order of the gratings acts as a mirror. Unlike gratings in zero order, prisms do not have an angle at which all wavelengths retro-reflect, and white light fringes cannot be used to set the ZPD in the interferometer. Therefore, other approaches to set ZPD were attempted, including using a Hg lamp and a pseudo-broadband source.

Figure 4.5 shows the emission spectrum of a low pressure Hg lamp with a spectral resolution of 0.46 nm, which was approximately three times higher than the theoretical resolution 0.14 nm. However, the Raman spectrum of CCl_4 was measured with the same system, and the spectrum was poorly resolved and had low signal-to-noise, as seen in Figure 4.6. Using the Hg lamp to set ZPD did not work, because the coherence length of the narrow emission lines is about 20 times longer than that of a typical Raman band (10 cm^{-1}). Therefore, a source with a larger spectral width than Raman bands was necessary to set the ZPD, so a 20 nm broadband filter centered around 558 nm was used to shorten the spectral range of a white light source. The spectrum of the 20 nm broadband source is shown in Figure 4.5 inset. Although the broadband source was resolved by the system, the fringe image had only a few fringes in the center portion, and the base thickness of the prism was thought to be increasing the wavefront error and degrading the fringe

image quality. The 30-60-90 coated-prism was the smallest apex angle prism with a mirror-coated back commercially available. Therefore, the coated-prisms were replaced by prism-mirror pairs to reduce the thickness of the prism and to use the mirrors to set the ZPD.

4.3.2 All-refractive SHRS Prototype 2

The second proto-type (Figure 4.1, (b.)) used right angle wedge prisms paired with mirrors, so the zero path difference could be set using the mirrors. The placement of the prism was arbitrary, with respect to zero path difference, along the z-axis, and only needed to be considered in terms of spectral range, meaning the distance between the mirror and prism should not be too great that the light reflected off the mirror did not travel back through the prism.

Using the mirrors to set ZPD was found to not work with the large apex angle prisms in the prism-mirror all-refractive SHRS design, because the mirrors had to be offset from the optical axis for geometric reasons and could not be used to set the ZPD. Therefore, smaller apex angle prisms (wedge prisms, ThorLabs # PS811) were used, which decreased dispersion and resolution. The final design of second prototype used a 7.68° apex angle prism and 1.27 cm entrance aperture, giving a theoretical resolving power of ~1370. Figure 4.7 shows the Hg emission spectrum measured using a prism-mirror pair all-refractive SHRS, and the measured resolution was ~2.4 nm, which was ~6 times larger than theoretical resolution.

Although the resolution was lower in the prism-mirror all-refractive SHRS, there were a few benefits to the decreased dispersion. The angles of the light exiting the prism

were smaller, allowing the mirrors to remain on the optical axis, and the mirrors could be used to set ZPD. The small apex angle prism could be treated as a thin prism, which means that a larger range of wavelengths exit the prism at about the same angle and should reduce loss in spectral range due to geometric concerns.

Separating the prism from the mirror increased the degrees of freedom that had to be controlled. The mirrors could be aligned along the optical easily by back reflection using the laser, and white light was used to set ZPD. Back reflection could not be used to align to the prisms due to the anti-reflection coating. The prisms were aligned along the optical axis using a target overlaid on the prisms. However, there was no clear way to precisely aligning the prisms in the xy plane to match one another exactly. Unlike a diffraction grating, prisms are not one dimensional, and the thickness of the prism increases from the apex angle to the base of the prism, see Figure 4.8. The prisms in each arm of the interferometer must be positioned precisely the same in the xy rotation plane to maintain a path difference between the two arms below the coherence length of a typical Raman band. If the rotation of the two prisms in the xy plane are more than 2° different, then the difference in pathlength between the two arms will be larger than the coherence length necessary from Raman measurements. With the mounts available, the xy plane rotation alignment had to be done by hand, and the required precision was not achieved.

4.4 Conclusions and Future Work

The all-refractive SHRS was demonstrated as a feasible instrument for emission measurements, but measuring Raman spectra proved more difficult. Alignment of the

prism-mirror pair all-refractive SHRS required many degrees of freedom of adjustment which increased the difficulty of alignment and reduced the quality of results, in comparison to the coated-prism SHRS. To continue the work on the all-refractive SHRS, future work should use the coated-prism design to decrease alignment issues. The main alignment issue stalling the progress of the all-refractive SHRS is setting the zero path difference. Several other contributing factors to the inability to measure Raman spectra with the all-refractive SHRS were difficulties making and maintaining alignment of the collection optics and stability issues caused by the opto-mechanical parts. The current grating SHRS uses high quality opto-mechanical parts that greatly reduced the stability issues, and these should be used for the all-refractive SHRS.

Future work should focus on determining a method for setting ZPD. A possible solution for setting ZPD with the coated-prism all-refractive SHRS would be to align the interferometer using gratings or mirrors in place of the prisms, and once the ZPD is aligned, put the prisms back in the system. The proposed method was one that was considered previously, but the inability precisely and repeatedly replace the prism impeded the process. The interferometer alignment was also hindered by the inadequate positioning of the prism on the center of rotation, because when a prism not centered over the rotation axis and is rotated, the ZPD between the two interferometer arms is lost. The grating mounts currently being used in the grating SHRS position the optic over the axis of rotation, which would be useful for the prism based SHRS.

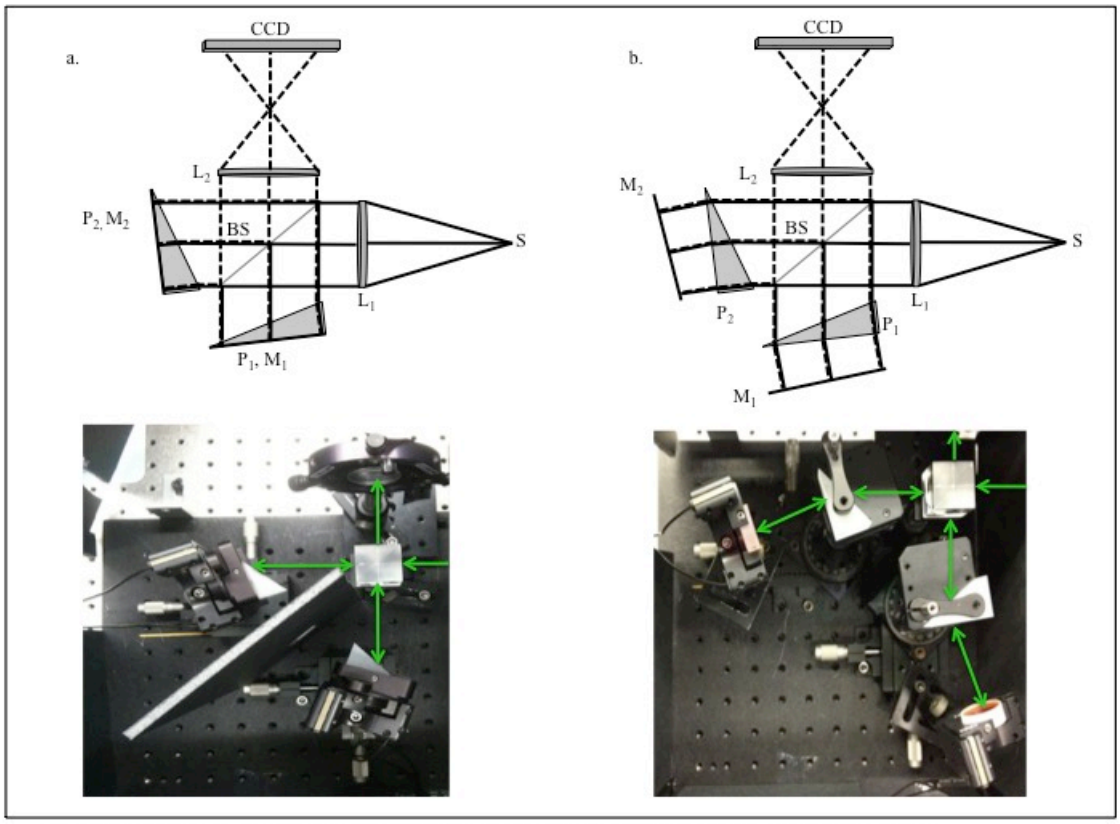

Figure 4.2: Schematic and images of proto-types built in our lab of an all-refractive SHRS in a mirror coated prism configuration (a.) and a prism mirror pair configuration (b.). S is the incoming signal, L_1 & L_2 are Lenses, BS is the beamsplitter,

Figure 4.1: Schematic and images of proto-types built in our lab of an all-refractive SHRS in a mirror coated prism configuration (a.) and a prism mirror pair configuration (b.). S is the incoming signal, L_1 & L_2 are Lenses, BS is the beam splitter, P_1 & P_2 are prisms, M_1 & M_2 are mirrrors, and the CCD is the detector. The Littrow angle is θ_L, and F are laser-blocking and bandpass filters

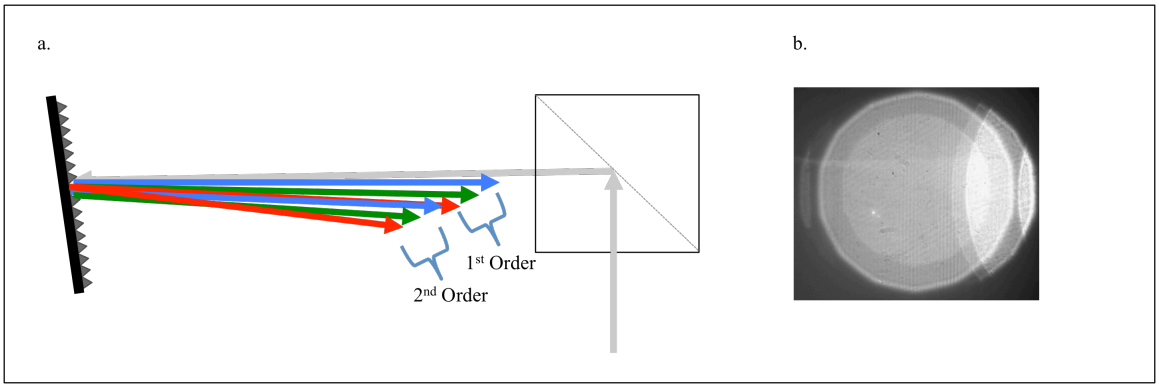

Figure 4.2: Schematic of order overlap (a.) and an image showing order overlap. Image is a fringe image recorded on the CCD in a grating-based SHRS system.

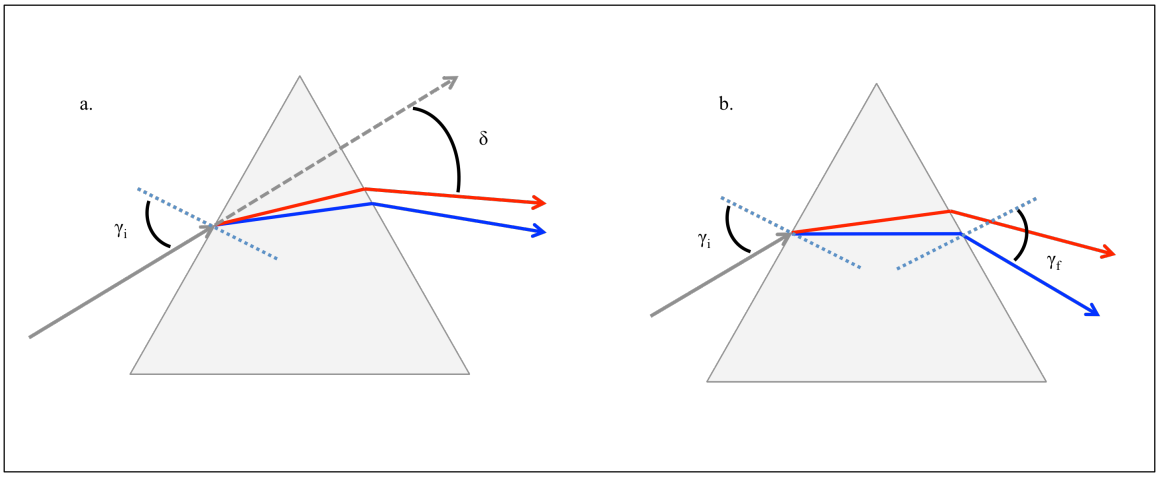

Figure 4.3: Schematic of dispersion in a prism showing the (a.) angle of deviation, δ, and (b.) a prism set to minimum deviation for blue light. Light blue dotted line is the normal to prism face, γ_i is the incident angle, and γ_f is the exit angle.

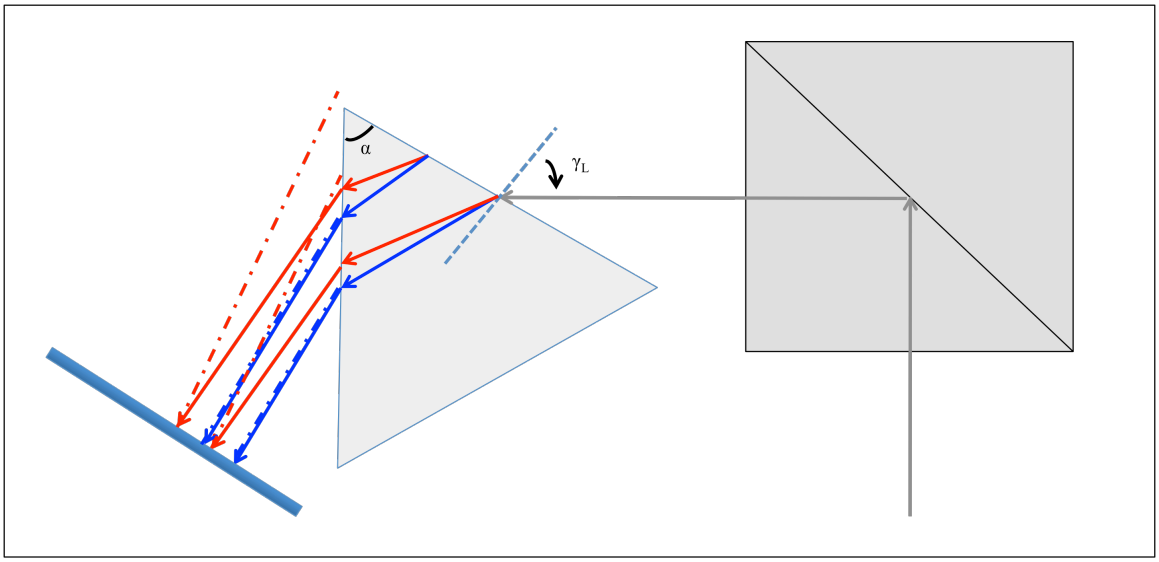

Figure 4.4: Schematic showing the dispersion through the prism. Angle of incidence (γ_L) and apex angle (α).

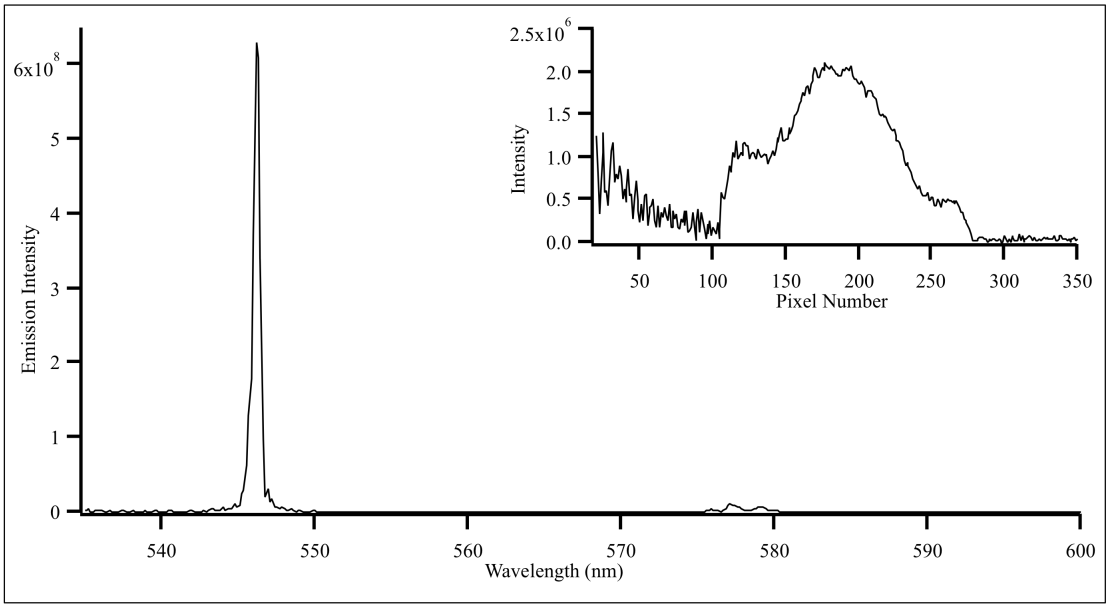

Figure 4.5: Emission spectrum from low pressure Hg lamp measured for 500 msec using the coated-prism all-refractive SHS set at 532 nm Littrow wavelength. Inset is a spectrum of a 20 nm broadband source (white light lamp filtered by a 558 nm bandpass filter) measured for 10 msec. acquisition time.

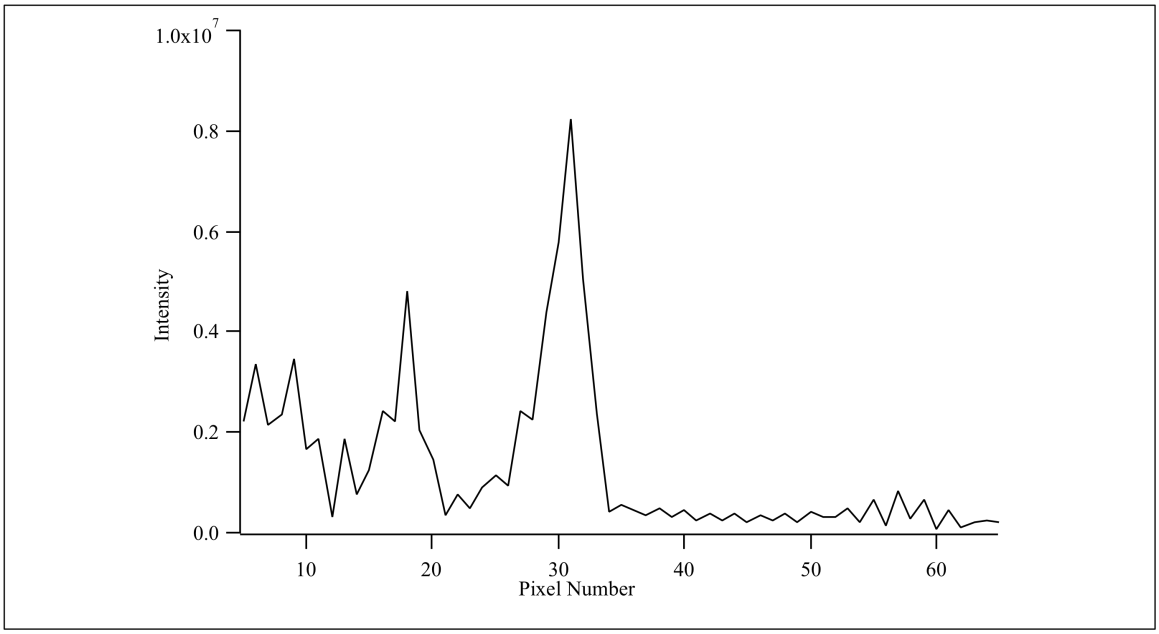

Figure 4.6: Raman spectrum of CCl_4 measured for 60 sec using the coated-prism all-refractive SHS set at 532 nm Littrow wavelength.

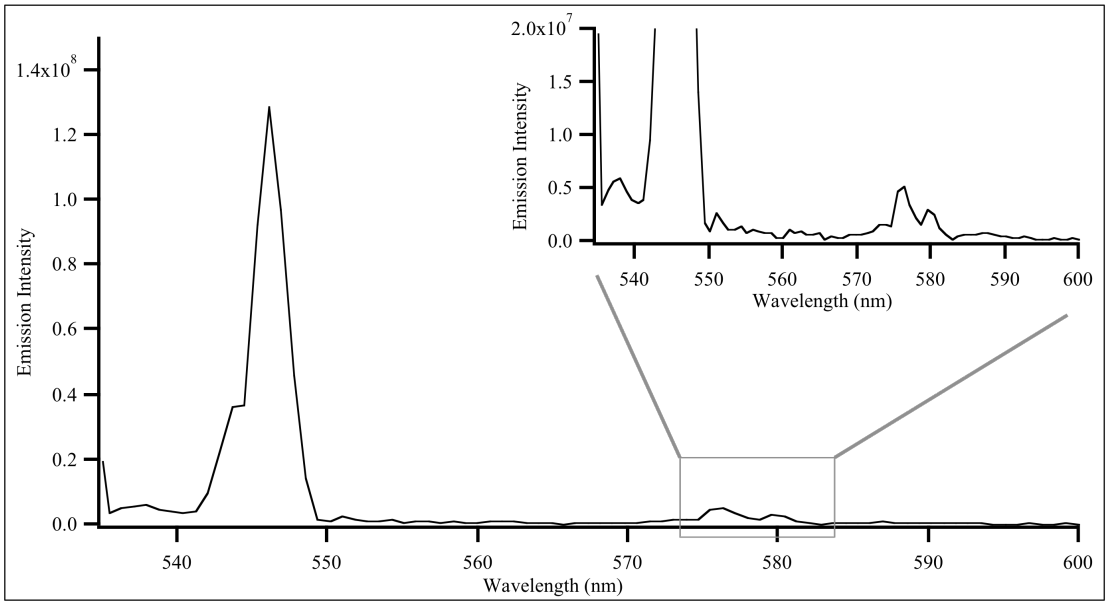

Figure 4.7: Emission spectrum from low pressure Hg lamp measured for 30 sec. acquisition time using the prism-mirror pair all-refractive SHS set at 532 nm Littrow wavelength. Inset is a same spectrum with y-axis scale change to show 576.9 and 579 nm emission lines.

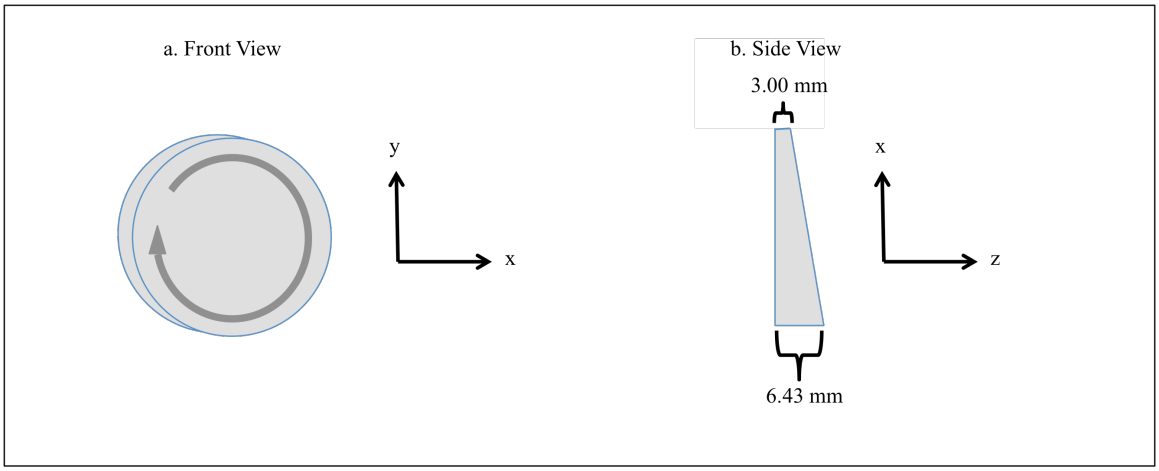

Figure 4.8: Illustration of the wedge prism (a) showing the rotation in the xy plane that affects the path difference in the two arms of the interferometer and (b.) showing the dimensions of the prism from a side view.

4.5 References

1. J.M. Harlander, C.R. Englert. Refractive Spatial Heterodyne Spectrometer. US Patent US20090231592 A1. Filed 2008. Issued 2009.
2. R.W. Wood. Physical Optics. 3rd ed. New York, USA: The McMillan Company
3. I.R. Kenyon. The Light Fantastic: A Modern Introduction to Classical and Quantum Optics. 2nd ed. New York, USA: Oxford University Press Inc., 2011.
4. F.S. Crawford, jr. Waves: Berkeley Physics Course Volume 3. USA: McGraw-Hill, 1968.

REFERENCES

1. A. Chopelas. “Single Crystal Raman Spectra of Forsterite, Fayalite, and Monticellite.” Am. Mineral. 1991. 76(7-8): 1101-1109.
2. A. Jubert, M.L. Legarto, N.E. Massa, L.L. Tevez, N.B. Okulik. “Vibrational and Theoretical Studies of Non-steroidal Anti-inflammatory Drugs Ibuprofen [2-(4-isobutylphenyl) propionic acid]; Napoxen [6-methoxy-α-methyl-2-naphthalene acetic acid] and Tolmetin Acids [1-methyl-5-(4methylbenzoyl)-1H-pyrrole-2-acetic acid]. J. Mol. Struct. 2006. 783(1-3): 34-5.
3. A. Pettersson, S. Wallin, H. Ostmark, A. Ehlerding, I.Johansson, M. Nordberg, H. Ellis, A. Al-Khalili. ‘‘Explosives Standoff Detection using Raman Spectroscopy: from Bulk Towards Trace Detection.’’ Proc. SCIE. 2010.76641K: 1–12.
4. A. Wang, R.L. Korotev, B.L. Jolliff, Z. Ling. “Raman Imaging of Extraterrestrial Materials.” Planet. Space Sci. 2015. 112(July 2015): 23-34.
5. A.J. Hobro, B. Lendl. “Stand-off Raman Spectroscopy.” Trends Anal. Chem. 28(11): 1235-1242.
6. B.W. Smith, J.M. Harlander. “Imaging Spatial Heterodyne Spectroscopy: Theory and Practice.” Proc. SPIE. 1999. 3698: 925-930.
7. C. Eliasson, N.A. Macleod, L.C. Jayes, F.C. Clarke, S.V. Hammond, M.R. Smith, P. Matousek. “Non-invasive Quantitative Assessment of the Content of

8. Pharmaceutical Capsules Using Transmission Raman Spectroscopy.” J. Pharm. Biomed. Anal. 2008. 47(2): 221-229.
9. C. Shantakumari. “Raman Spectra of Crystalline Sulphates of Zinc, Magnesium and Sodium.” P. Indian. As-Math. Sci. 1953. 37(3): 393-400.
10. C.P. Marshall, A.O. Marshall. “Challenges Analyzing Gypsum on Mars by Raman Spectroscopy.” Astrobiology 2015. 15(9): 761-769.
11. C.V. Raman, K.S. Krishnan. “A New Type of Secondary Radiation”. Nature. 1928. 121(3048): 501–502.
12. D. Oelkrug, E. Ostertag, R.W. Kessler. “Quantitative Raman Spectroscopy in Turbid Matter: Reflection or Transmission Mode?” Anal. Bioanal. Chem. 2013. 405(10): 3367-3379.
13. D. Oelkrug, M. Brun, P. Hubner, K. Rebner, B. Boldrini, R.W. Kessler. “Penetration of Light into Multiple Scattering Media: Model Calculations and Reflectance Experiments. Part II: the Radial Transfer. Appl. Spectrosc. 2012. 66(8): 934-943.
14. D.A. Leonard. ‘‘Observation of Raman Scattering from the Atmosphere using a Pulsed Nitrogen Ultraviolet Laser.’’ Nature. 1967. 216(5111): 142–143.
15. D.B. Chase. “Fourier Transform Raman Spectroscopy.” J. Am. Chem. Soc. 1986. 108(24): 7485-7488.
16. E.L. Izake. “Forensic and Homeland Security Applications of Modern Porable Raman Spectroscopy.” Forensic Sci. Int. 2010. 202(1-3): 1-8.

17. F. Hanke, U. Bottger, S.G. Pavlov, H.-W. Hubers. ‘‘Raman Spectra of Frozen Salt Solutions Relevant for Planetary Surfaces.’’ EPSC Abstracts. 2014. 9(EPSC2014): 403-1.
18. F.S. Crawford, jr. Waves: Berkeley Physics Course Volume 3. USA: McGraw-Hill, 1968.
19. G. Hu, W. Xiong, H. Shi, Z. Li, J. Shen, X. Fang. “Raman Spectroscopic Detection for Liquid and Solid Targets using a Spatial Heterodyne Spectrometer.” J. Raman Spectrosc. 2016. 47(3): 289-298.
20. G. Hu, W. Xiong, H. Shi, Z. Li, J. Shen, X. Fang. “Raman Spectroscopic Detection using Two-Dimensional Spatial Heterodyne Spectrometer.” Opt. Eng. 2015. 54(11): 114101-1 - 114101-9.
21. I. Durickovic, R. Claverie, P. Bourson, M. Marchetti, J.-M. Chassot, M.D. Fontana. “Water-ice Phase Transition Probed by Raman Spectroscopy.” J. Raman Spectrosc. 2011. 42(6): 1408-1412.
22. I.R. Kenyon. The Light Fantastic: A Modern Introduction to Classical and Quantum Optics. 2nd ed. New York, USA: Oxford University Press Inc., 2011.
23. J. Cooney. ‘‘Satellite Observations Using Raman Component of Laser Backscatter.’’ In: R. Zirkind (ed.) Proceedings of the Symposium of Electromagnetic Sensing of the Earth from Satellites. New York, NY: Polytechnic Institute of Brooklyn Press, 1967, pp. P1–P10.
24. J. Harlander, R. Reynolds, F. Roesler. “Spatial Heterodyne Spectroscopy for the Exploration of Diffuse Interstellar Emission-Lines at Far-Ultraviolet Wavelengths.” Astrophys. J. 1992. 396(2): 730-740.

25. J. Johansson, A. Sparen, O. Svensson, S. Folestad, M. Claybourn. “ Quantitative Transmission Raman Spectroscopy of Pharmaceutical Tablets and Capsules.” Appl. Spectrosc. 2007. 61(11): 1211-1218.

26. J. Moros, J.A. Lorenzo, K. Novotny´, J.J. Laserna. ‘‘Fundamentals of Stand-off Raman Scattering Spectroscopy for Explosive Fingerprinting.’’ J. Raman Spectrosc. 2013. 44(1): 121–130.

27. J.C. Carter, J. Scaffidi, S. Burnett, B. Vasser, S.K. Sharma, S.M. Angel. ‘‘Stand-off Raman Detection using Dispersive and Tunable Filter Based Systems.’’ Spectrochim. Acta, Part A. 2005. 61(10): 2288–2298.

28. J.C. Carter, S.M. Angel, M. Lawrence-Snyder, J. Scaffidi, R.E. Whipple, J.G. Reynolds. ‘‘Standoff Detection of High Explosive Materials at 50 Meters in Ambient Light Conditions Using a Small Raman Instrument.’’ Appl. Spectrosc. 2005. 59(6): 769–775.

29. J.F. Scott, S.P.S. Porto. “Longitudinal and Transverse Optical Lattice Vibrations in Quartz.” Phys. Rev. 1967. 161(3): 903-910.

30. J.J. Laserna, editor. Modern Techniques in Raman Spectroscopy. New York, USA: Wiley, 1993.

31. J.M. Harlander, C.R. Englert. Refractive Spatial Heterodyne Spectrometer. US Patent US20090231592 A1. Filed 2008. Issued 2009.

32. J.M. Harlander, F.L. Roesler, J.G. Cardon, C.R. Englert, R.R. Conway. “Shimmer: A Spatial Heterodyne Spectrometer for Remote Sensing of Earth’s Middle Atomsphere.” Appl. Opt. 2002. 41(7): 1343-1352.

33. J.M. Harlander, F.L. Roesler, S. Chakrabarti. “Spatial Heterodyne Spectroscopy: A Novel Interferometric Technique for the FUV.” In: O.H.W. Siegmund, H.S. Hudson, editors. EUV, X-Ray, and Gamma-Ray Instrumentation for Astronomy. Proc. SPIE. 1990, 1344: 120-131.

34. J.M. Harlander. Spatial Heterodyne Spectroscopy: Interferometric Performance at any Wavelength Without Scanning. [Ph.D. Thesis]. Madison, WI: University of Wisconsin, 1991.

35. K. Shin, H. Chung. “ Wide Area Coverage Raman Spectroscopy for Reliable Quantitative Analysis and its Applications.” Analyst 2013. 138(12): 3335-3346.

36. K.A. Horton, N. Domergue-Schmidt, S.K. Sharma, P. Deb, P.G. Lucey. ‘‘Remote Raman System for Planetary Landers: Data Reduction and Analysis.’’ Paper presented at: LPSC 2000.Houston, TX; March 13–17 2000.

37. K.B. Mabrouk, T.H. Kauffman, H. Aroui, M.D. Fontana. “Raman Study of Cation Effect on Sulfate Vibration Modes in Solid State and in Aqueous Solutions.” J. Raman Spectrosc. 2013. 44(11): 1603-1608.

38. K.L. Gares, K.T. Hufziger, S.V. Bykov, S.A. Sanford. “Review of Explosive Detection Methodologies and the Emergence of Standoff Deep UV Resonance Raman.” J. Raman Spectrosc. 2016. 47(1): 124-141.

39. M. Gaft, L. Nagli. ‘‘UV Gated Raman Spectroscopy for Standoff Detection of Explosives.’’ Opt. Mater. 2008. 30(11): 1739–1746.

40. M. Ghosh, L. Wang, S.A. Asher. ‘‘Deep-Ultraviolet Resonance Raman Excitation Profiles of NH4NO3, PETN, TNT, HMX, and RDX.’’ Appl. Spectrosc. 2012. 66(9): 1013–1021.

41. M. Prencipe, F. Pascale, C.M. Zicovich-Wilson, V.R. Sanders, R. Orlando, R. Dovesi. “The Vibrational Spectrum of Calcite (CaCO3): an ab initio Quantum-Mechanical Calculation.” Phys. Chem. Minerals 2004. 31(8): 559-564.
42. M. Skulinova, C. Lefebvre, P. Sobron, E. Eshelman, M. Daly, J.-F. Gravel, J.F. Cormier, F. Chaˆteauneuf, G. Slater, W. Zheng, A. Koujelev, R. Leveille. ‘‘Time-resolved Stand-off UV-Raman Spectroscopy for Planetary Exploration.’’ Planet. Space Sci. 2014. 92: 88–100.
43. M. Wu, M. Ray, K.H. Fung, M.W. Ruckman, D. Harder, A.J. Sedlacek. ‘‘Stand-off Detection of Chemicals by UV Raman Spectroscopy.’’ Appl. Spectrosc. 2000. 54(6): 800–806.
44. M.D. Ray, A.J. Sedlacek, M. Wu. ‘‘Ultraviolet Mini-Raman Lidar for Stand-off, In Situ Identification of Chemical Surface Contaminants.’’ Rev. Sci. Instrum. 2000. 71(9): 3485–3489.
45. M.J. Pelletier, P. Larkin, M. Santangelo. “Transmission Fourier Transform Raman Spectroscopy of Pharmaceutical Tablet Core.” Appl. Spectrosc. 2012. 66(4): 451-457.
46. M.J. Pelletier. “Sensitivity-Enhanced Transmission Raman Spectroscopy.” Appl. Spectrosc. 2013. 67(8): 829-840.
47. N. Everall, I. Priestnall, P. Dallin, J. Andrews, I. Lewis, K. Davis, H. Owen, M.W. George. “Measurement of Spatial Resolution and Sensitivity in Transmission and Backscattering Raman Spectroscopy of Opaque Samples: Impact on Pharmaceutical Quality Control and Raman Tomography.” Appl. Spectrosc. 2010. 64(5): 476-484.

48. N. Everall, P. Matousek, N. MacLeod, K.L Ronayne, I.P. Clark. “Temporal and Spatial Resolution in Transmission Raman Spectroscopy.” Appl. Spectrosc. 2010. 64(1): 52-60.

49. N. Everall, T. Hahn, P. Matousek, A. W. Parker, M. Towrie. “Picosecond Time-Resolved Raman Spectroscopy of Solids: Capabilities and Limitations for Fluorescence Rejection and the Influence of Diffuse Reflectance.” Appl. Spectrosc. 2001. 55(12): 1701–1708.

50. N. Lamsal, S. K. Sharma, T. E. Acosta, S. M. Angel. “Ultraviolet Stand-off Raman Measurements Using a Gated Spatial Heterodyne Raman Spectrometer.” Appl. Spectrosc., in press 2016, DOI: 10.1177/0003702816631304.

51. N. Lamsal, S. M. Angel, S. K. Sharma, T. E. Acosta. “Visible and UV Standoff Raman Measurements in Ambient Light Conditions Using a Gated Spatial Heterodyne Raman Spectrometer”. Abstract 1459, 46th LPSC 2015. Woodland TX; March 16-20, 2015.

52. N. Lamsal, S.M. Angel. ‘‘Deep-Ultraviolet Raman Measurements Using a Spatial Heterodyne Raman Spectrometer (SHRS).’’ Appl. Spectrosc. 2015. 69(5): 525–534.

53. N. Stone, P. Matousek. “Advanced Transmission Raman Spectroscopy: A Promising Tool for Breast Disease Diagnosis.” Cancer Res. 2008. 68(11): 4424-4430.

54. N.A. Macleod, P. Matousek. “Emerging Non-invasive Raman Methods in Process Control and Forensic Applications.” Pharmaceut. Res. 2008. 25(1): 2205-2215.

55. N.R. Gomer, C.M. Gordon, P. Lucey, S.K. Sharma, J.C. Carter, S.M. Angel. "Raman Spectroscopy Using a Spatial Heterodyne Spectrometer: Proof of Concept." Appl. Spectrosc. 2011. 65(8): 849-857.
56. P. D. Barnett, N. Lamsal, S. M. Angel. "Standoff LIBS using a Miniature Wide Field of View Spatial Heterodyne Spectrometer with Sub-Microsteradian Collection Optics." Appl. Spectrosc. Submitted for publication February 2016.
57. P. Matousek, A.W. Parker. "Bulk Raman Analysis of Pharmaceutical Tablets." Appl. Spectrosc. 2006. 60(12): 1353-1357.
58. P. Matousek. "Raman Signal Enhancement in Deep Spectroscopy of Turbid Media." Appl. Spectrosc. 2007. 61(8): 845-854.
59. P.G. Lucey, T.F. Cooney, S.K. Sharma. ''A Remote Raman Analysis System for Planetary Landers.'' Paper presented at: LPSC 1998. Houston, TX; March 16–20 1998.
60. R. Savoie, P. Beauchesne, D. Levesque. "Fourier Transform Raman Spectroscopy in the Visible Region." Microchim. Acta. 1988. 95(1): 223-225.
61. R.J. Bakker. "Raman Spectra of Fluid and Crystal Mixtures in the Systems H2O, H2O-NaCl and H2O-MgCl2 at Low Temperatures: Applications to Fluid-Inclusion Research." Can. Mineral. 2004. 42(5): 1283-1314.
62. R.L. Aggarwal, L.W. Farrar, D.L. Polla. ''Measurement of the Absolute Raman Scattering Cross Sections of Sulfur and the Standoff Raman Detection of a 6 mm thick Sulfur Specimen at 1500 m.'' J. Raman Spectrosc. 2011. 42(3): 461–464.

63. R.L. McCreery. ‘‘Magnitude of Raman Scattering.’’ In: T.D. Winefordner (ed.) Raman Spectroscopy for Chemical Analysis. New York, NY: John Wiley & Sons, Inc, 2000, pp.15–33.
64. R.L. McCreery. “CCD Array Detectors for Multichannel Raman Spectroscopy.” In: J. Sweedler, K. Ratzlaff, and M.B. Denton, editors. Charge Transfer Devices in Spectroscopy. New York, USA: VCH, 1994. Pp. 227-228.
65. R.L. McCreery. Raman Spectroscopy for Chemical Analysis. New York, USA: Wiley, 2000.
66. R.M. Measures. Laser Remote Sensing: Fundamentals and Applications. New York, USA: John Wiley & Sons, 1984.
67. R.S. Das, Y.K. Agrawal. “Raman Spectroscopy: Recent Advancements, Techniques and Applications.” Vib. Spectrosc. 2011. 57(2): 163-176.
68. R.W. Wood. Physical Optics. 3rd ed. New York, USA: The McMillan Company
69. S.A. Asher, C.R. Johnson. ‘‘Raman Spectroscopy of a Coal Liquid Shows that Fluorescence Interference is Minimized with Ultraviolet Excitation.’’ Science. 1984. 225(4659): 311–313.
70. S.A. Asher. ‘‘UV Resonance Raman Spectroscopy for Analytical, Physical, and Biophysical Chemistry. Part 1.’’ Anal. Chem. 1993. 65(2): 59A–66A.
71. S.K. Sharma, P.G. Lucey, M. Ghosh, H.W. Hubble, K.A. Horton. “Stand-off Raman spectroscopic Detection of Minerals on Planetary Surfaces.” Spectrochim. Acta, Part A. 2003. 59(10): 2391-2407.

72. S.M. Angel, N.R. Gomer, S.K. Sharma, C. McKay. ‘‘Remote Raman Spectroscopy for Planetary Exploration: A Review.’’ Appl. Spectrosc. 2012. 66(2): 137–150.

73. S.M. Angel, T.J. Kulp, T.M. Vess. ‘‘Remote-Raman Spectroscopy at Intermediate Ranges Using Low-Power CW Lasers.’’ Appl. Spectrosc. 1992. 46(7): 1085–1091.

74. S.P. Mulvaney, C.D. Keating. “Raman Spectroscopy.” Anal. Chem. 2000. 72(12): 145-158.

75. T. Hirschfeld, B. Chase. “FT-Raman spectroscopy: Development and Justification.” Appl. Spectrosc. 1986. 40(2): 133-136.

76. T. Hirschfeld. ‘‘Range Independence of Signal in Variable Focus Remote Raman Spectrometry.’’ Appl. Opt. 1974. 13(6): 1435–1437.

77. T.J. Kulp, S.E. Bisson, T.A. Reichardt. ‘‘Standoff Ultraviolet Raman Scattering Detection of Trace Levels of Explosives.’’ Sandia Natl. Lab. [Tech. Rep.] Sandia Report. 2011. 7955. doi:10.2172/1030305.

APPENDIX A: PERMISSION TO REPRINT

Copyright Permissions for Chapter 3: K.A. Strange, K.C. Paul, S.M. Angel. "Transmission Raman Spectroscopy using a Spatial Heterodyne Raman Spectrometer (SHRS)." Applied Spectrosc. In press, March 2016.

Dear K. Alicia Strange Fessler,

Thank you for your email. I am pleased to report we can grant your request without a fee as part of your dissertation.

Please accept this email as permission for your request as detailed below. Permission is granted for the life of the edition on a non-exclusive basis, in the English language, throughout the world in all formats provided full citation is made to the original SAGE publication. As your article has been accepted but not yet published, we request that you include "in press" in your article's citation.

The permission is subject to approval from any co-authors on the original project. Please note approval excludes any graphs, photos, excerpts, etc. which required permission from a separate copyright holder at the time of publication. If your material includes anything which was not your original work, please contact the rights holder for permission to reuse those items.

Please let me know if you should have any further questions.

Best Wishes,

Craig Myles
on behalf of **SAGE Ltd. Permissions Team**

SAGE Publishing
1 Oliver's Yard, 55 City Road
London, EC1Y 1SP
UK
www.sagepublishing.com